TU Delft

Delft University of Technology

Document Version
Final published version

Licence
Dutch Copyright Act (Article 25fa)

Citation (APA)
Sadeghi, S. M. M., Aghajani, H., Jalilvand, H., Ahmady-Asbchin, S., Sadati, S. M., Coenders-Gerrits, M., & Dymond, S. F. (2026). Canopy vitality drives rainfall redistribution in an old-growth temperate beech forest. *Forest Ecology and Management*, *606*, Article 123552. https://doi.org/10.1016/j.foreco.2026.123552

Important note
To cite this publication, please use the final published version (if applicable).
Please check the document version above.

Copyright
In case the licence states “Dutch Copyright Act (Article 25fa)”, this publication was made available Green Open Access via the TU Delft Institutional Repository pursuant to Dutch Copyright Act (Article 25fa, the Taverne amendment). This provision does not affect copyright ownership.
Unless copyright is transferred by contract or statute, it remains with the copyright holder.

Sharing and reuse
Other than for strictly personal use, it is not permitted to download, forward or distribute the text or part of it, without the consent of the author(s) and/or copyright holder(s), unless the work is under an open content license such as Creative Commons.

Takedown policy
Please contact us and provide details if you believe this document breaches copyrights.
We will remove access to the work immediately and investigate your claim.

*This work is downloaded from Delft University of Technology.*

Forest Ecology and Management 606 (2026) 123552

Contents lists available at ScienceDirect

Forest Ecology and Management

journal homepage: www.elsevier.com/locate/foreco

# Canopy vitality drives rainfall redistribution in an old-growth temperate beech forest

Seyed Mohammad Moein Sadeghi [a,*], Hamed Aghajani [b,*], Hamid Jalilvand [b], Salman Ahmady-Asbchin [c], Seyed Mazyar Sadati [d], Miriam Coenders-Gerrits [e], Salli F. Dymond [a]

[a] School of Forestry, Northern Arizona University, Flagstaff, AZ, USA
[b] Department of Forest Sciences and Engineering, Sari Agricultural Sciences and Natural Resources University, Sari, Iran
[c] Department of Microbiology, Faculty of Science, University of Mazandaran, Babolsar, Iran
[d] Department of Plant Protection, Sari Agricultural Sciences and Natural Resources University, Sari, Iran
[e] Department of Water Management, Faculty of Civil Engineering and Geosciences, Delft University of Technology, Delft, the Netherlands

ARTICLE INFO

*Keywords:*
Canopy vitality
*Fagus orientalis*
Forest disturbance
Forest health
Iran
Rainfall interception
Stemflow
Throughfall

ABSTRACT

Forest disturbance increasingly manifests not only through abrupt events such as fire or windthrow, but also through progressive canopy vitality decline driven by pathogens, stress, and mortality—processes that fundamentally reorganize forest structure and function. The ecohydrological consequences of such vitality-driven disturbance remain poorly understood in old-growth temperate forests. This study examined how progressive canopy deterioration—from healthy crowns to branchless snags—affects rainfall partitioning and canopy hydrological parameters in an old-growth Hyrcanian oriental beech (*Fagus orientalis* Lipsky) forest of northern Iran. Over one full hydrological year, fifteen trees were randomly selected to represent five vitality stages and were instrumented to measure throughfall, stemflow, and interception under both leaf-on and leafless conditions. A reformulated Gash analytical model (RGAM) was applied to simulate interception dynamics. Results revealed that throughfall increased as both interception and stemflow declined systematically with decreasing canopy vitality, indicating a transition from hydrologically buffered to more transmissive canopy conditions. Nonetheless, snag trees exhibited measurable rainfall interception—7.9 % for branched and 2.8 % for branchless snags—challenging the assumption that snags contribute negligibly to canopy evaporation. Stemflow generation decreased sharply as crown connectivity deteriorated and was consistently lower in the leafless period. RGAM accurately reproduced interception for healthy and moderately degraded trees but overestimated losses in severely deteriorated canopies, suggesting that model parameters must account for canopy heterogeneity and vitality-dependent storage dynamics. These findings provide the first quantitative assessment of rainfall redistribution across a five-stage canopy vitality gradient, explicitly including both branched and branchless snags, demonstrating that canopy degradation substantially alters rainfall storage, channeling, and evaporation processes. Incorporating tree vitality and deadwood structure into interception modeling will improve predictions of rainfall redistribution, soil moisture, and water yield in old-growth and uneven-aged temperate forests worldwide.

## 1. Introduction

Rainfall partitioning by forest canopies, through processes of interception, throughfall, and stemflow, plays a pivotal role in regulating ecosystem water balances (Yue et al., 2021), soil moisture dynamics (Fischer-Bedtke et al., 2023), nutrient fluxes (Grundmann et al., 2024), and forest–atmosphere exchanges (Lian et al., 2022; Xu, 2023). These processes not only influence groundwater recharge and surface runoff (Tang, 1996) but also mediate energy fluxes (Chen et al., 2019; Coenders-Gerrits et al., 2020), thereby affecting local- to regional-scale climate feedbacks (Miralles et al., 2025). Rainfall partitioning is widely recognized as a function of meteorological conditions (e.g., wind speed

* Corresponding authors.
*E-mail addresses:* s.sadeghi@nau.edu (S.M.M. Sadeghi), h.aghajani@sanru.ac.ir (H. Aghajani).

https://doi.org/10.1016/j.foreco.2026.123552
Received 10 December 2025; Received in revised form 15 January 2026; Accepted 17 January 2026
Available online 27 January 2026
0378-1127/© 2026 Elsevier B.V. All rights are reserved, including those for text and data mining, AI training, and similar technologies.

and vapor pressure deficit), stand structural parameters (e.g., canopy cover, leaf area index, basal area), and rainfall properties (e.g., magnitude and intensity) (Sadeghi et al., 2020). In the context of climate change, however, declining tree health and increased mortality are becoming more frequent across temperate forests (Etemad, et al., 2025), amplifying the need to understand how canopy health modulates hydrological processes. Changes in tree vitality—from healthy crowns to partial dieback and eventual mortality—can alter canopy storage, drip points, and the routing of water along bark surfaces, thereby reshaping the balance among interception, throughfall, and stemflow (Sadeghi et al., 2023). Yet, little attention has been given to how these vitality-driven changes modify rainfall partitioning, particularly in temperate forests.

The specific mechanisms by which tree crown decline alters rainfall partitioning are increasingly evident. Defoliation, whether driven by seasonality (Herbst et al., 2008; Mużyło et al., 2012) or crown diseases (Jeong and Otsuki, 2021; Sadeghi et al., 2023; Spittlehouse and Maloney, 2023), combined with progressive dieback, reduces canopy storage capacity and aerodynamic roughness (Maurer et al., 2013), typically decreasing interception loss and increasing throughfall amounts (Sadeghi et al., 2023). Pathogen- or insect-induced foliage thinning can further shift raindrop size distributions beneath the canopy (Levia et al., 2017), thereby altering raindrop kinetic energy and enhancing splash erosion potential (Jeong et al., 2024). As canopy decline advances, branch loss and crown breakage disrupt drip points and stem connectivity, producing highly variable stemflow responses. Some studies report reduced stemflow in small declining trees, where diminished crown area limits the capacity to channel water toward the bole (Sadeghi et al., 2023). In contrast, medium-sized trees may exhibit elevated stemflow because crown simplification concentrates precipitation into fewer but more efficient flow paths, while bark characteristics still favor water channeling (Sadeghi et al., 2023). These changes in stemflow dynamics not only alter the spatial pattern of infiltration but can also influence near-stem erosion, sediment movement, and small-scale runoff generation within forests. These contrasting findings highlight that the relationship between canopy decline and stemflow is fundamentally nonlinear and strongly context-dependent, mediated by interactions among tree size, crown architecture, and bark traits. At advanced stages, bark softening, decay, and epiphyte colonization may either enhance or impede stemflow depending on alterations in bark roughness, hydrophobicity, and macro-channel continuity (Levia and Germer, 2015; McGee et al., 2019; Tonello et al., 2021). Ultimately, standing dead trees (snags) have reduced evaporative surfaces and canopy storage but retain trunks that may shed rainfall inefficiently. However, empirical evidence on how snags influence rainfall partitioning remains limited, and available studies suggest that effects on throughfall, stemflow, and interception are highly context-dependent rather than generalizable (Waiters and Price, 1988; Jeong and Otsuki, 2021). Existing research has primarily relied on binary or disturbance-based contrasts, including comparisons of burned versus unburned areas (Mitsudera et al., 1984; Su et al., 2022), diseased versus healthy trees or stands (Sadeghi et al., 2023), drought-declined versus non-declined trees (Rodrigues et al., 2021), and stands that have been thinned or partially harvested versus unthinned controls (Mazza et al., 2011; Hakimi et al., 2018; Dietz et al., 2006). However, few studies have explicitly stratified trees into discrete vitality stages (Sadeghi et al., 2023) to quantify rainfall partitioning along a continuous health gradient, particularly in temperate broadleaf systems.

Temperate broadleaf forests play a critical role in regional and global carbon and water cycles (Roberts, 2009; Panahandeh et al., 2022), yet the hydrological implications of progressive canopy vitality decline in these ecosystems remain poorly understood. This knowledge gap is particularly relevant in forest systems increasingly exposed to multiple stressors. The Hyrcanian temperate forests in northern Iran, a UNESCO World Heritage site (Keybondori et al., 2025), provide a particularly important context as they are dominated by oriental beech (*Fagus orientalis* Lipsky) (Sagheb-Talebi et al., 2014; Azaryan et al., 2025), a keystone species that is increasingly threatened by fungal pathogens (Zamani et al., 2024), insect outbreaks (Farashiani et al., 2023), drought stress (Saeedi et al., 2022), and windstorms (Abdi et al., 2020). Notably, these forests retain key old-growth characteristics, including large, uneven-aged trees, high structural complexity, and abundant snags (standing deadwoods) (Sagheb-Talebi et al., 2014; Azaryan et al., 2025), making them an ideal system for examining how long-term canopy vitality gradients influence rainfall partitioning. Beyond the Hyrcanian region, oriental beech also occurs in several temperate regions of southeastern Europe, including Bulgaria, Greece, and Turkey (Kohler et al., 2024), where it grows under warmer and drier conditions than its close relative, European beech (*Fagus sylvatica*) (Mellert and Šeho, 2022). This broader climatic distribution suggests that certain provenances exhibit comparatively greater drought tolerance, highlighting the importance of understanding how vitality loss influences key ecosystem processes under future climate change scenarios. Against this backdrop of increasing disturbance pressure and structural heterogeneity, we distinguished five canopy vitality stages—healthy trees, fungus-infected, top-dry individuals (trees that remain alive but have lost their upper crown due to dieback), branched snags, and branchless snags—to capture the full continuum of vitality loss within oriental beech. Consistent with this vitality-based framework, national and international conservation guidelines emphasize that the retention of declining and dead standing trees—such as top-dry individuals, fungus-infected trees, and snags—is essential for improving microhabitat conditions (Sefidi and Copenheaver, 2020), maintaining structural complexity and enhancing biodiversity within protected temperate forests (Alavi et al., 2020; Sefidi, 2023).

This management-driven recognition of canopy vitality diversity highlights that rainfall partitioning should be assessed along a continuous gradient from full vigor to complete mortality, rather than as a simple contrast between live and dead trees. This perspective is increasingly embedded in close-to-nature silvicultural practices through the deliberate retention and monitoring of dead and dying trees, reflecting their importance for biodiversity (Jörg et al., 2016), carbon storage (Tavankar et al., 2022), and long-term forest ecosystem resilience (Kooch et al., 2023; Jahdi et al., 2023). By explicitly incorporating multiple canopy vitality stages, our study provides a conceptually and methodologically novel framework for quantifying how canopy decline reshapes hydrological processes in temperate forests, while directly linking rainfall partitioning to conservation-oriented forest management strategies.

Quantifying rainfall partitioning across gradients of canopy vitality requires approaches that can effectively isolate the effects of structural decline from event-scale meteorological variation—an inherently difficult task in field settings. Because partitioning is strongly shaped by forest structure, storm characteristics, and their interactions, direct observations are often limited to specific locations or short monitoring periods. Analytical and process-based models therefore provide an essential complement, allowing canopy interception and related fluxes to be explored across a broader range of rainfall regimes and canopy configurations. Among these, the reformulated Gash analytical model (RGAM; Gash et al., 1995; Valente et al., 1997) is especially relevant in declining canopies because it incorporates partial wetting and event-scale evaporation dynamics, processes that become increasingly important as canopy storage capacity and crown connectivity diminish. Although simplified, RGAM has been successfully applied across a wide range of forest types (Muzylo et al., 2009; Sadeghi et al., 2017; Panahandeh et al., 2022; Sadeghi et al., 2024; Melo Neto et al., 2024; Ma et al., 2025), and even within agricultural systems (Nazari et al., 2020).

This study aims to (i) quantify rainfall partitioning (throughfall, stemflow, and canopy interception) across five distinct canopy vitality stages of oriental beech in the Hyrcanian temperate forest, (ii) evaluate how progressive canopy vitality decline, from full vigor to complete mortality, alters the balance among these fluxes across both leaf-on

(leafed) and leafless phenological periods, and (iii) assess the performance of RGAM across contrasting and increasingly simplified canopy conditions. We hypothesize that (H1) rainfall partitioning differs between leaf-on and leafless periods, with pronounced contrasts among canopy vitality stages emerging in the leaf-on season but largely converging toward similar responses in the leafless season when foliage is absent; (H2) during the leaf-on season, the four non-fully foliated stages (i.e., fungus-infected, top-dry, and branched and branchless snags) show distinct and systematically altered throughfall, interception, and stemflow patterns compared to healthy trees, reflecting differences in crown integrity, bark condition, and dominant water redistribution pathways; and (H3) the predictive performance of RGAM declines with canopy deterioration, as reductions in canopy storage and hydrological drainage connectivity increasingly challenge the underlying model assumptions.

## 2. Material and methods

### 2.1. Study area and tree selection

The experimental plots were established in parcels 14 and 15 of District 1 in the Darabkola Forests of northern Iran (near the city of Sari), at elevations of 420–440 m a.s.l. (36°46′74″–36°55′57″ N, 53°27′09″–53°33′19″ E). The Darabkola Forest is part of the Neka Choob Company managed area. Geologically, the region was formed during the Tertiary period of the Cenozoic Era. The soils are classified as forest brown soils, with textures ranging from moderately heavy (clay–loam) to heavy (silty–clay). Slopes generally face north to northwest (Anonymous, 2008). The climate is humid temperate (Csa, Köppen classification), with hot, dry summers and mild, wet winters (Raziei, 2022). Meteorological data from the newly established Darabkola Rainfall Station (2021; 36°46′74″–36°55′57″ N, 53°27′09″–53°33′19″ E, elevation 425 m a.s.l.), located < 500 m west of the study site, indicate a mean annual precipitation of 1400 mm/year for the period 2020–2024, of which approximately 93 % falls as rain and the remainder as snow. Because this station provides only short-term records, we used data from the Sari Synoptic Meteorological Station (distance ca. 22 km; 36°32′08″ N, 52°59′55″ E, elevation: 17 m a.s.l.) to place our study period in a long-term climatic context (1999 −2024). Air temperature shows pronounced seasonality, ranging from a maximum of 32 °C in July to a minimum of −17 °C in January. In this study, reference evapotranspiration ($ET_0$) was calculated using the FAO-56 Penman–Monteith (Allen et al., 1998) method based on meteorological data from the Sari Synoptic Meteorological Station.

The forest canopy is dominated by oriental beech (*Fagus orientalis* Lipsky), forming a typical Hyrcanian beech-dominated community. Oriental beech was selected for this study because it is the second most widespread tree species in the Hyrcanian temperate forest (Sagheb-Talebi et al., 2014) and dominates the study parcel, representing approximately 85 % of the studied stand. To assess the effects of canopy health on rainfall partitioning, we modified the vitality classification of Aghajani et al. (2018), which originally comprised four categories, by adding an additional distinction within snag class. Specifically, we differentiated branched snags (standing dead trees retaining branches but no foliage) and branchless snags (standing dead trees reduced to the trunk only). Thus, five distinct canopy vitality stages were recognized in this study (Fig. 1; Table 1), each defined by distinct structural and physiological characteristics. Together, these stages represent a progressive gradient from full vigor to complete mortality and allow evaluation of how crown deterioration modifies canopy eco-hydrological processes. For each canopy vitality stage, three open-grown, solitary mature trees were randomly selected as study individuals, with maturity defined as a diameter at breast height (DBH, 1.3 m above ground) of 45–65 cm (Král et al., 2010). To minimize edge and competition effects, all sampled trees were located within the overstory layer, and none experienced canopy overlap from surrounding trees (Owens et al., 2006). Given the close proximity among individuals (maximum separation of 250 m), meteorological conditions were considered spatially uniform across the study area.

In June 2024, structural attributes were measured for all sampled trees. DBH was recorded using a Haglöf Mantax Blue caliper (Sweden). Tree height and crown length ($C_l$)—measured from the lowest primary branch to the crown apex—were obtained using an ultrasonic hypsometer (Forester Vertex type III, Sweden). Crown width ($C_w$) was determined by measuring the horizontal distance from the trunk to the outermost shoot projection in eight cardinal and intercardinal directions using a measuring tape (±0.1 m accuracy). The mean $C_w$ was then calculated as the quadratic mean of the eight crown diameter measurements. Bark thickness (mm) was measured at DBH by carefully piercing the bark and recording its thickness with a ruler (±1 mm accuracy).

**Table 1**
Tree vitality stages and field criteria used to classify oriental beech (*Fagus orientalis*) in the Darabkola Forest, Northern Iran.

| Canopy vitality stages | Definition |
|---|---|
| Healthy | Fully foliated, dense green crowns with no visible dieback, discoloration, or crown thinning. |
| Fungus-infected | Partial crown dieback affecting about 15–25 % of the canopy, characterized by patchy defoliation, reduced foliage density, irregular branching, and visible fungal signs such as fruiting bodies or lesions. |
| Top-dry | Severe crown dieback affecting roughly 30–40 % of the canopy, with the upper crown completely dead and containing broken or dry branches, while the lower crown retains some living foliage; overall crown structure is vertically simplified. |
| Branched snag | Standing dead tree retaining most branches and crown architecture but completely defoliated; bark often decayed, shedding, or colonized by epiphytes or fungi. |
| Branchless snag | Standing dead trunk (bole) with no remaining major branches, representing an advanced decay stage and complete canopy loss. |

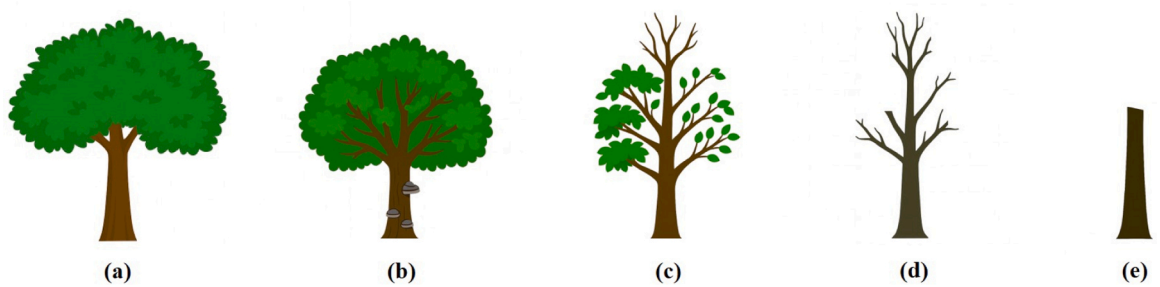



**Fig. 1.** Schematic representation of the five canopy vitality stages of oriental beech (*Fagus orientalis*) used in this study: (a) healthy, (b) fungus-infected, (c) top-dry, (d) branched snag, and (e) branchless snag. Explanations of each class are provided in Table 1.

### 2.2. Measurements of canopy rainfall partitioning

Gross rainfall ($P_g$) and rainfall partitioning across the five canopy vitality stages were monitored on an event basis over one full year, from 1st May 2024 to 30 April 2025. $P_g$ was measured using three plastic, funnel-type manual rain gauges, complemented by a standard manual rain gauge installed at the Darabkola Precipitation Station, approximately 400 m from the experimental plots. Manual gauges correlated closely with the tipping-bucket gauge at the station, as indicated by the strong linear relationship ($P_{g_manual} = 0.98\,P_{g_standard} - 0.03$) with a high coefficient of determination ($R^2 = 0.97$) based on 27 rainfall events ($n = 27$). This strong agreement confirms the reliability of the manual funnel-type gauges, which were subsequently used for this study. All gauges were installed in open areas and positioned at angles less than 45° from the nearest treetop to minimize canopy interference (Sadeghi et al., 2017). $P_g$ events were defined as storms delivering more than 0.5 mm of precipitation, consistent with on-site observations and previous studies in the region (Nezamdoost et al., 2018; Panahandeh et al., 2022).

Throughfall ($T_f$) was collected using twelve fixed collectors per tree, identical to those used for $P_g$, arranged randomly beneath the crown in the four cardinal directions ($n = 36$ $T_f$ collectors per canopy vitality stage; n = 180 $T_f$ collectors in total). Because branchless snags lack a functional crown, collectors were installed around the bole to characterize rainfall reaching the forest floor within the trunk-influenced zone, including both direct precipitation and any redistribution by the dead stem. We acknowledge that near-bole placement may slightly reduce measured $T_f$ relative to positions farther from the stem; however, this placement reflects the dominant redistribution pathway for branchless snags and does not affect comparisons among vitality stages because of the consistent sampling design applied across all storm events.

Stemflow ($S_f$) was collected using collars constructed from clear vinyl tubing, which were wrapped twice around each tree and installed at a slight downward angle to facilitate drainage (Sadeghi et al., 2017). The inner edges of the collars were stapled to the trunk and sealed with 100 % silicone to ensure a watertight attachment. Each collar was connected to three 20-L polyethylene reservoirs. $S_f$ depth was calculated by converting collected $S_f$ volume to depth using an appropriate collection area. For live trees and branched snags, $S_f$ depth was obtained by dividing $S_f$ volume by crown projection area (CPA), estimated from the horizontal projection of the remaining canopy structure. For branchless snags, where no functional crown exists, bole diameter was measured at the uppermost remaining point of each snag, basal area was calculated from this diameter, and this area was used as a proxy for the collection area to convert $S_f$ volume to $S_f$ depth. All $P_g$, $T_f$, and $S_f$ collectors were regularly inspected and cleaned to prevent blockages from dirt, debris, leaves, or insects. To reduce evaporation losses during rainfall intervals, $T_f$ and $S_f$ were measured manually from the gauges as soon as possible, typically within 2 h after rainfall ceased. The amount of canopy interception ($I$, mm) was estimated following a simple water-balance approach, in which the difference between gross rainfall ($P_g$) and the total water reaching the forest floor as throughfall ($T_f$) and stemflow ($S_f$):

$$I = \quad P_g - \left(T_f + S_f\right) \tag{1}$$

### 2.3. Canopy phenological stage

Throughout the study period, rainfall events were classified into two canopy phenological stages: the leaf-on period (1 May–5 November 2024 and 28 March–30 April 2025) and the leafless period (6 November 2024–27 March 2025). The onset of the leafless stage was defined as the date on which complete leaf fall had occurred, verified through weekly phenological observations at the site. For branched and branchless snags, classification by phenological stage is not ecologically meaningful, as these trees remain leafless throughout the year. To maintain consistency in statistical comparisons, snag measurements were assigned to the corresponding phenological stages defined for the living trees.

### 2.4. Reformulated Gash analytical model (RGAM)

The RGAM requires several canopy- and trunk-scale ecohydrological parameters for its application. Among these, the crown saturation threshold ($P'_g$),—the rainfall depth needed to fill the crown storage capacity ($S$)— was determined as the inflection point ($I_p$) in the relationship between $T_f$ ($y$-axis) and $P_g$ ($x$-axis) compiled from all monitored events (following the approach of Pypker et al., 2005). According to this threshold, rainfall events were classified as pre-saturation or post-saturation, with separate linear regressions fitted for each condition ($R_1$ and $R_2$, respectively). $R_1$ describes canopy dynamics prior to saturation, while $R_2$ characterizes canopy behavior after saturation. By definition, $P'_g$ is always equal to or greater than $S$. It becomes equivalent to $S$ only under conditions where the free throughfall coefficient ($p$) approaches zero—representing a fully closed canopy—and when evaporation losses during the wetting phase are negligible. The parameter $S$ was defined as the maximum volume of water retained by the canopy once saturation was reached (Van Dijk et al., 2015), estimated from the $x$-intercept of the $R_2$ regression (Gash et al., 1995). The slope of $R_1$ was interpreted as the free throughfall coefficient ($p$), representing the proportion of $P_g$ that bypasses canopy interception and reaches the forest floor directly (Gash et al., 1995). The wet-canopy evaporation ratio ($\bar{E}/\bar{R}$) was calculated as one minus the slope of $R_2$, representing the proportion of rainfall lost to evaporation relative to total precipitation intensity.

Stemflow dynamics were parameterized following the approach of Gash and Morton (1978). The stemflow partitioning coefficient ($p_t$) and trunk storage capacity ($S_t$) were derived from the linear regression of stemflow ($S_f$, $y$-axis) against gross rainfall ($P_g$, $x$-axis), using the slope and intercept, respectively, as model parameters. The coefficient $p_t$ represents the proportion of rainfall diverted along the stem surface, whereas $S_t$ defines the maximum volume of water that can be held on the trunk before additional rainfall contributes to $S_f$ generation. The trunk saturation threshold ($P''_g$), defined as the minimum rainfall depth required to saturate the trunk, i.e., the rainfall needed to fill $S_t$, was calculated as $S_t/p_t$, where $pt$ is the stemflow partitioning coefficient. Thus, $P''_g$ is directly analogous to $P_g$ for the canopy, with $S_t$ representing the trunk counterpart of $S$.

Finally, canopy interception capacity ($I$) was calculated using the RGAM (Eq. 2).

$$\sum_{j=1}^{n+m} I_j = c\sum_{j=1}^{m} P_{g,j} + c\left[\sum_{j=1}^{n} P'_{g,j} + \frac{\bar{E}_C}{\bar{R}}\sum_{j=1}^{n}\left(P_{g,j} - P'_{g,j}\right)\right] + qS_{tc} + p_{tc}\left[1 - \frac{\bar{E}_C}{\bar{R}}\right]\sum_{j=1}^{n-q}\left(P_{g,j} - P'_{g,j}\right) \tag{2}$$

In this formulation, $P_g$ events are divided into those that do not saturate the canopy ($m$ events) and those that do ($n$ events). For each rainfall event ($j$), canopy interception loss ($I$) is represented as the sum of three physically based components: (i) the rainfall fraction required to wet the canopy before saturation, (ii) the additional rainfall received once the canopy is saturated, adjusted for canopy evaporation ($\bar{E}_c/\bar{R}$), and (iii) the contribution from trunk storage and stemflow pathways. Here, $j$ denotes individual storm events, $q$ represents the number of $P_g$ storms that lead to full trunk saturation, $S_{tc}$ is the trunk storage capacity normalized by canopy area, and $p_{tc}$ denotes the stemflow partitioning coefficient expressed per unit canopy area. Based on field observations, canopy drying was assumed to require at least 4 h under sunny conditions and up to 6 h under cloudy conditions, ensuring that successive events were treated as hydrologically independent.

### 2.5. Statistical analysis and model performance evaluation

The normality of the data was tested using the Kolmogorov–Smirnov test. To compare rainfall partitioning among the five canopy vitality stages, we used one-way analysis of variance (ANOVA). When significant differences were detected, Tukey's honest significant difference (HSD) test ($p < 0.05$) was applied as a post hoc multiple-comparison procedure to identify pairwise differences among canopy vitality stages in percentage relative throughfall ($T_f/P_g$ (%); i.e., the percentage of throughfall per rainfall event), percentage relative stemflow ($S_f/P_g$ (%)), and percentage relative canopy interception ($I/P_g$ (%)). To characterize how $P_g$ relates to canopy fluxes, we fit nonlinear exponential models, as percentage relative rainfall partitioning—throughfall ($T_f/P_g$ (%)), stemflow ($S_f/P_g$ (%)), and interception ($I/P_g$ (%))—arises from a markedly skewed, non-uniform temporal distribution of rainfall and inherently nonlinear partitioning processes (e.g., Lloyd, 1990; Sadeghi et al., 2024). For both percentage relative throughfall ($T_f/P_g$ (%)) and percentage relative stemflow ($S_f/P_g$ (%)) we used a cumulative exponential model of the form:

$$F(x) = a - be^{(-cx)} \quad (3)$$

which increases toward an upper asymptote $a$ ($< 1.0$), starting from an initial offset defined by $a - b$. To ensure physically meaningful and bounded results, we constrained the fitted values of $T_f/P_g$ (%) and $S_f/P_g$ (%) to lie between 0 % and 100 % by applying lower and upper bounds during post-processing of the model output. For percentage relative canopy interception ($I/P_g$ (%)), we used an exponential decay model of the form:

$$F(x) = a + be^{(-cx)} \quad (4)$$

which declines toward an asymptote $a$. When $a = 0$, this simplifies to $F(x) = be^{(-cx)}$, approaching zero asymptotically as rainfall amount increases. To avoid non-physical negative predictions, any model outputs less than zero were set to zero. Non-linear regressions were fitted using the "drc" package in R (Ritz and Streibig, 2005). Model performance was evaluated using the root mean square error (*RMSE*), coefficient of determination ($R^2$), and Nash–Sutcliffe efficiency (*NSE*; Nash and Sutcliffe, 1970).

All analyses were conducted at three temporal scales—the leaf-on period, leafless period, and annual period (see 2.3 for definitions)—to account for seasonal variability in each canopy condition. All statistical analyses were performed in R (version 3.6.1).

## 3. Results

### 3.1. Canopy structural parameters

Structural attributes of the sampled oriental beech trees differed systematically across canopy vitality stages despite comparable DBH values (Table 2). Crown dimensions (height, width, and projection area) and bark thickness declined progressively from healthy to fungus-infected and top-dry trees, with branchless snags retaining only the bole structure and showing the lowest bark thickness (Table 2). The slenderness coefficient (tree height/DBH) averaged 44.4, 42.3, and 40.9 for healthy, fungus-infected, and top-dry trees, respectively, all within the range of mechanically stable trees (<80; Wang et al., 1998). Branchless snags showed the lowest slenderness coefficient (20.2) because tree height was substantially reduced while DBH remained relatively large (Table 2). This suggests that although crown vitality stages influenced crown architecture and bark traits, the sampled trees were comparable in terms of mechanical stability, with snags exhibiting the greatest structural resistance due to their low height-to-diameter ratio.

### 3.2. Long-term mean and observed meteorological data

Monthly climate conditions during the study year differed notably from the long-term average (Fig. 2). Precipitation (Fig. 2a) was highly variable, with a pronounced peak in November (261 mm/month) that exceeded the long-term mean, whereas the early spring months (January–March) received below-average precipitation. The mean long-term annual precipitation was 780 mm/year, while the study year received 1027 mm/year (~30 % higher). Air temperature (Fig. 2b) generally followed the long-term seasonal pattern, with only minor deviations; the mean long-term annual temperature was 17.2 °C, compared with 18.4 °C in the study year. Reference evapotranspiration ($ET_o$; Fig. 2c) increased steadily from winter to summer, reaching a maximum of > 5 mm day$^{-1}$ in July before declining toward winter. The mean long-term annual $ET_o$ was 2.54 mm day$^{-1}$ , whereas the study year averaged 2.87 mm day$^{-1}$ (~13 % higher). $ET_o$ during the study year was consistently higher than the long-term average, except in November, indicating comparatively drier atmospheric conditions for most of the year.

**Table 2**
Structural characteristics of oriental beech (*Fagus orientalis*) trees across five canopy vitality stages in the Darabkola Forest, northern Iran. Values in parentheses indicate standard errors (± SE).

| Canopy vitality stage | Number of trees | DBH (cm) | Tree height (m) | Crown height ($C_h$; m) | Crown width ($C_w$; m) | $C_h$:$C_w$ | Crown projection area (m$^2$) | Slenderness coefficient (–) | Bark thickness (cm) |
|---|---|---|---|---|---|---|---|---|---|
| Healthy | 3 | 54.0 (± 3.3) | 23.6 (± 1.6) | 11.2 (± 0.8) | 7.0 (± 0.3) | 1.62 (± 0.18) | 38.7 (± 3.6) | 44.4 (± 4.8) | 3.11 (± 0.25) |
| Fungus-infected | 3 | 53.3 (± 0.7) | 22.5 (± 1.1) | 8.1 (± 0.5) | 8.1 (± 0.5) | 1.21 (± 0.12) | 36.1 (± 2.8) | 42.3 (± 2.1) | 2.61 (± 0.08) |
| Top-dry | 3 | 57.0 (± 4.1) | 23.0 (± 0.8) | 6.5 (± 0.2) | 6.7 (± 0.2) | 0.98 (± 0.04) | 35.4 (± 2.3) | 40.9 (± 2.4) | 2.59 (± 0.18) |
| Branched snag | 3 | 53.7 (± 2.4) | 17.2 (± 0.9) | 3.2 (± 0.4) | 3.0 (± 0.4) | 0.79 (± 0.03) | 14.0 (± 1.6) | 32.3 (± 2.6) | 1.63 (± 0.23) |
| Branchless snag | 3 | 53.3 (± 3.7) | 10.8 (± 1.0) | 0 | 0 | 0 | 0 | 20.2 (± 0.9) | 0.63 (± 0.16) |

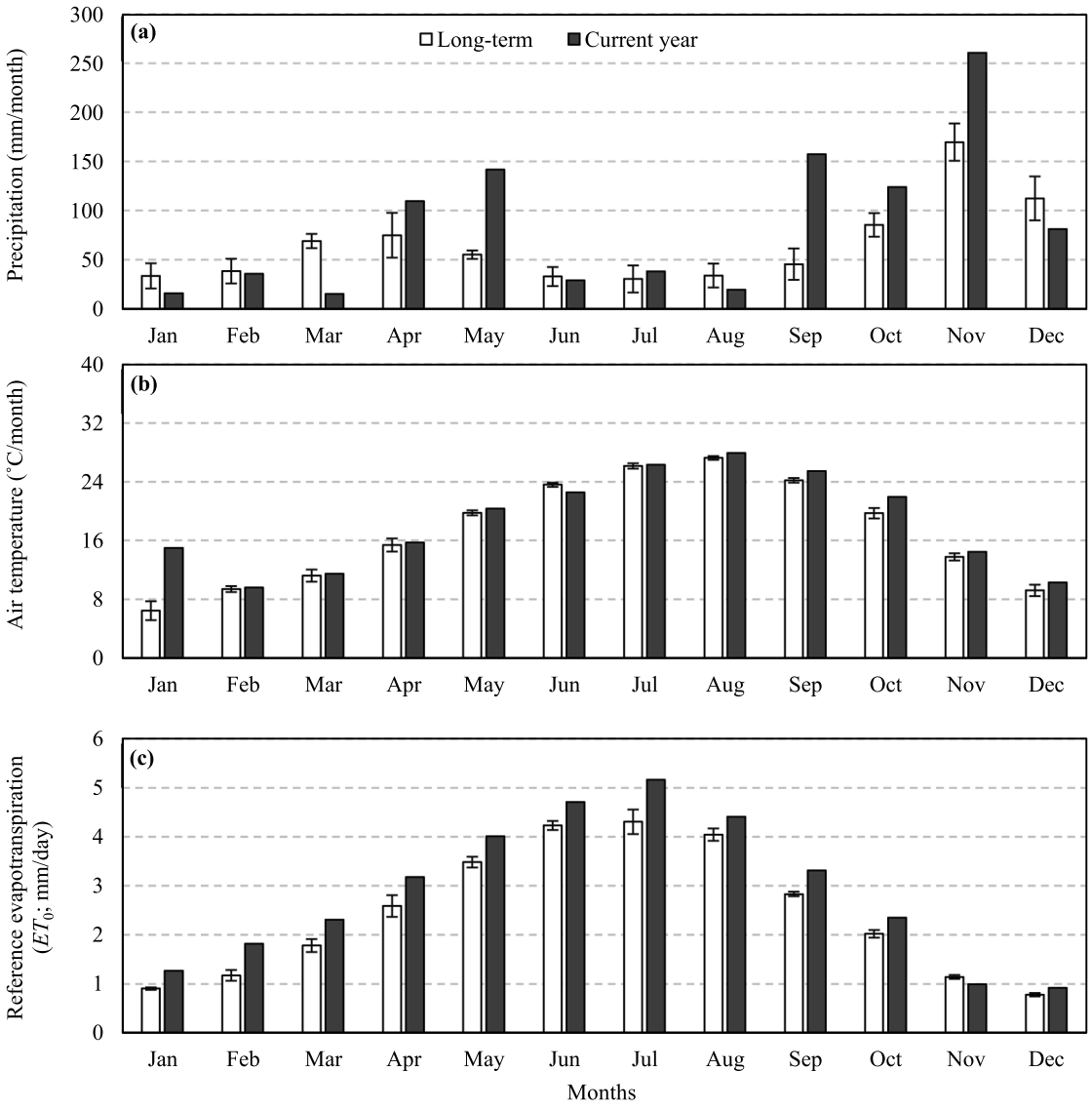



**Fig. 2.** Monthly variations in (a) precipitation, (b) air temperature, and (c) reference evapotranspiration ($ET_0$) for the study site. Bars represent the long-term average (open bars) and the study year (filled bars; June 2024 to May 2025). Error bars denote standard errors of the long-term mean.

**Table 3**
Summary statistics of gross rainfall ($P_g$) events by phenoseasons and the annual period.

| Phenological scale | $P_g$ amount | | | | | |
|---|---|---|---|---|---|---|
| | n | Mean (mm) | Median (mm) | Max (mm) | Min (mm) | SE ( ±mm) |
| Leaf-on | 45 | 14.09 | 9.55 | 59.96 | 0.64 | 2.26 |
| Leafless | 32 | 12.28 | 3.41 | 74.32 | 0.58 | 3.01 |
| Annual | 77 | 13.34 | 6.45 | 74.32 | 0.58 | 1.82 |

### 3.3. Gross rainfall ($P_g$)

A total of 77 discrete storm events were recorded during the study period across all treatments. $P_g$ magnitudes ranged from 0.6 mm to 74.3 mm. Storm frequency differed between phenoseasons, with more events recorded during the leaf-on period ($n = 45$) than during the leafless period ($n = 32$). The annual mean $P_g$ was 13.3 ± 1.8 mm per event, with phenoseason-specific means of 14.1 ± 2.3 mm for the leaf-on period and 12.3 ± 3.0 mm for the leafless period (Table 3). Rainfall characteristics varied markedly across storm size classes and phenological periods (Fig. S1). Small storms (≤ 2.5 mm) dominated in frequency during both phenoseasons, accounting for about 47 % of total storm occurrences in the leaf-on period (Fig. S1a) and ~31 % in the leafless period (Fig. S1b), yet they contributed less than 5 % of the total rainfall amount (Fig. S1a and S1b). In contrast, large storms (> 25 mm) were relatively infrequent—comprising only ~16 % of events during the leafless period (Fig. S1b) but nearly 24 % during the leaf-on period (Fig. S1a)—while supplying more than 64 % of the total rainfall. Intermediate storms (10.01–25.00 mm) represented 20–30 % of both storm frequency and rainfall volume, contributing moderately to total inputs. These results indicate that rainfall delivery was strongly skewed toward a small number of high-magnitude events, particularly during the leafless season (Fig. S1b), when large storms occurred more frequently and accounted for a greater proportion of annual rainfall.

### 3.4. Quantification of rainfall partitioning ($T_f$, $S_f$, and $I$) amounts

$T_f$ volumes did not differ significantly among tree vitality stages at the annual scale ($F = 0.36$, $p > 0.05$), during the leaf-on period ($F = 0.40$, $p > 0.05$), or during the leafless period ($F = 0.03$, $p > 0.05$) (Table S1). Although differences were not statistically significant,

branchless snags consistently exhibited the highest $T_f$ (13.9 mm in the leaf-on and 12.1 mm in the leafless periods), while healthy trees had the lowest $T_f$ (10.6 and 10.9 mm, respectively; Table S1). This represents a ~30 % higher $T_f$ in branchless snags compared to healthy trees. In contrast, $S_f$ volumes varied significantly with vitality stage during the annual period ($F = 12.27$, $p < 0.05$). Tukey's HSD test showed that $S_f$ volumes in snag treatments (both branched and branchless snags) were significantly lower than those in the other canopy vitality stages (Table S1). Healthy trees generated 1.07 mm of $S_f$ annually, ~36 times higher than branchless snags (average = 0.03 mm) (Table S1). Healthy trees yielded 1.29 mm $S_f$, which was approximately 43 times higher than branchless snags (average = 0.03 mm; Table S1). During the leafless period ($F = 3.03$, $p < 0.05$), healthy and fungus-infected trees also produced significantly greater $S_f$ than snags, with healthy trees generating 0.74 mm $S_f$ compared to 0.04 mm in branchless snags (~18-fold difference). $I$ also differed strongly among canopy vitality stages ($F = 51.77$, $p < 0.05$). Post-hoc comparisons indicated that $I$ in branched and branchless snags (0.22 and 0.15 mm, respectively) was significantly lower than in the other canopy vitality stages, while healthy trees showed the highest $I$ values (1.58 mm; Table S1). During the leaf-on period ($F = 62.19$, $p < 0.05$), healthy trees intercepted significantly more rainfall than all other canopy vitality stages, with 2.25 mm in healthy trees compared to 0.15 mm in branchless snags (~15-fold difference; Table S1). During the leafless period, $I$ remained significantly greater in healthy trees compared to the other stages ($F = 37.91$, $p < 0.05$; Table S1). For example, healthy trees intercepted 0.64 mm compared to 0.16 mm in branchless snags (~4-fold difference) during the leafless period (Table S1).

Event-based rainfall partitioning, expressed as percentage relative rainfall partitioning, differed strongly among canopy vitality stages and showed the same rank ordering during the leaf-on, leafless, and annual periods (Fig. 3; Table S2). $T_f/P_g$ (%) was greatest in branchless and branched snags, intermediate in top-dry and fungus-infected trees, and lowest in healthy trees across all study periods (Fig. 3; Table S2). Phenological effects were most pronounced in the living classes: $T_f/P_g$ (%) increased from the leaf-on to the leafless period in healthy, fungus-infected, and top-dry trees, whereas snags exhibited only minor changes across phenophases (Fig. 3a, d, and g; Table S2). The largest mean contrast in $T_f/P_g$ (%) occured between branchless snags and healthy trees (Table S2), reaching 40.2 % in the leaf-on period, 28.0 % in the leafless period, and 35.1 % at the annual period. $S_f/P_g$ (%) displayed the inverse ordering, with healthy > fungus-infected > top-dry > branched ~ branchless snags (Fig. 3b, e, and h; Table S2). $S_f/P_g$ (%) also declined from the leaf-on to the leafless period for all canopy vitality stages, most notably in healthy trees (Fig. 3b and e; Table S2). The largest mean contrast in $S_f/P_g$ (%) was between healthy and branchless snags (Table S2): 4.7 % in the leaf-on period, 2.1 % in the leafless period, and 3.6 % annual period. As a consequence, $I/P_g$ (%) was consistently higher in the living classes than in snags and tended to decrease from the leaf-on to the leafless period for the living classes, with only minor phenological shifts in snags (Fig. 3b, e, and h; Table S2). $I/P_g$ (%) mirrored these patterns (Fig. 3c, f, and i; Table S2): it was highest in the living

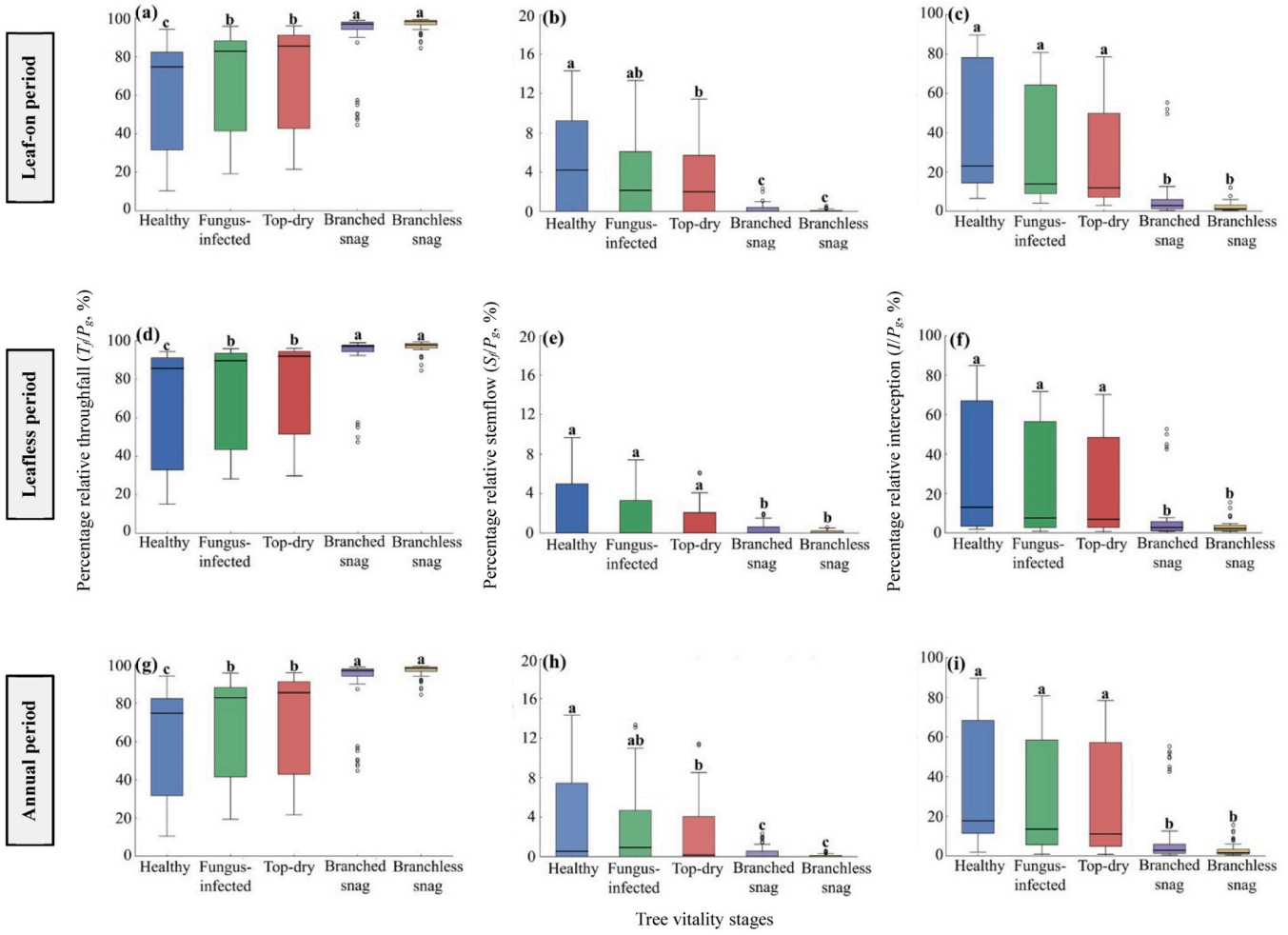



**Fig. 3.** Event-based rainfall partitioning (percentage relative throughfall, stemflow, and interception) by tree vitality stage. Panels (a–c) show the leaf-on period, (d–f) the leafless period, and (g–i) the annual period. Boxes show medians and interquartile ranges; whiskers = 1.5 ×IQR; open circles = outliers. Lowercase letters indicate Tukey HSD groupings (α = 0.05); shared letters = not significantly different.

classes (healthy > fungus-infected > top-dry) and lowest in both snag classes, with only minor phenological shifts in snags (Fig. 3c, f, and i; Table S2). $I/P_g$ (%) decreased from the leaf-on to the leafless period in the living classes (Fig. 3c and f). The largest mean contrast in $I/P_g$ (%) was between healthy and branchless snags: 35.4 % in the leaf-on period, 25.9 % in the leafless period, and 31.5 % annual scale (Table S2).

### 3.5. Relationship between rainfall amount and canopy rainfall partitioning

The relationships between $P_g$ amount and canopy water fluxes ($T_f$, $S_f$, and $I$) were well described by single-variable regression models across all canopy vitality stages and phenological periods (Tables S3–S5). Overall, $T_f$ increased nearly linearly with $P_g$ ($R^2 = 0.99$; Table S3), while $S_f$ (Table S4) and $I$ (Table S5) displayed greater variability ($R^2$ = 0.77–0.86 and 0.41–0.99, respectively). Distinct differences emerged between phenological stages (Table S3–S5). During the leaf-on period, $T_f$–$P_g$ relationships were slightly less steep (slopes 0.79–0.99) than during the leafless period (0.91–0.99) (Table S3). Conversely, $S_f$ during the leaf-on period required higher rainfall thresholds to initiate (6–15 mm) and showed stronger nonlinearity, especially in branched snags, compared to more linear $S_f$–$P_g$ relationships observed in the leafless period (Table S4). $I$ was highest and most variable during the leaf-on period, particularly in healthy trees ($I = 0.988 + 0.090P_g$; $R^2$ = 0.88), but declined sharply during the leafless period ($R^2 < 0.55$) (Table S5). Among canopy vitality stages, healthy and fungus-infected trees consistently intercepted more rainfall and generated higher $S_f$ volumes, whereas snags—especially branchless snags—showed near-complete rainfall transmission, as indicated by $T_f$ slopes close to unity (~ 0.99) and minimal interception losses (Tables S3–S5).

Because absolute canopy fluxes (mm/event; Tables S3–S5) reflect rainfall magnitude rather than proportional redistribution, we further examined the relative partitioning of $P_g$ into $T_f$%, $S_f$%, and $I$% to better capture the non-linear response of canopy rainfall dynamics across increasing $P_g$ amounts. The relationships between $P_g$ and $T_f/P_g$ (%) were well described by exponential functions across all canopy vitality stages and phenological periods (Fig. 4). During the leaf-on period (green curves; Fig. 4a, d, g, j, and m), $T_f/P_g$ (%) increased sharply with $P_g$ and approached an asymptote beyond ~5 mm. Model performance was strong, with $R^2$ values ranging from 0.63 to 0.91 and *RMSE* between 1.35 % and 9.60 % (Fig. 4a, d, g, j, and m). During the leafless period (purple curves; Fig. 4b, e, h, k, and n), $T_f/P_g$ (%) similarly followed an exponential trend with high model fits ($R^2$ = 0.78–0.91; *RMSE* = 1.62–9.43 %). For the overall study year (i.e., annual scale; gray curves; Fig. 4c, f, i, l, and o), the exponential models also provided satisfactory fits ($R^2$ = 0.68–0.85; *RMSE* = 1.60–13.95 %). Across all phenological periods, $T_f$% approached an upper asymptote near 95 % at higher rainfall amounts, and the fitted exponential functions consistently captured these asymptotic trends for each canopy vitality stage. The fitted exponential parameters showed that the intercept coefficient ($a$)—representing the asymptotic maximum of $T_f/P_g$ (%)—was generally highest during the leafless period (92.3–98.5; Fig. 4b, e, h, k, and n) and lowest during the leaf-on period (77.2–98.9; Fig. 4a, d, g, j, and m). The exponential rate coefficient ($b$), which controls the curvature and rate of increase in $T_f/P_g$ (%) with $P_g$, ranged from 0.43 to 3.30 across canopy vitality stages. The steepest $b$ values, indicating the most rapid initial increase of $T_f/P_g$ (%) with $P_g$ amount, were found in the snag treatments (Fig. 4j–n), while smaller $b$ values occurred in healthy and fungus-infected trees (Fig. 4a–f).

Exponential models effectively described the relationships between $P_g$ and $S_f$% across canopy vitality stages and phenological periods (Fig. 5). During the leaf-on period (green curves; Fig. 5a, d, g, j, and m), $S_f/P_g$ (%) exhibited a gradual increase with $P_g$, showing no clear saturation even at higher rainfall amounts. Model performance varied among vitality stages, with $R^2$ values between 0.53 and 0.86 and *RMSE* ranging from 0.10 % to 2.46 % (Fig. 5a, d, g, j, and m). During the leafless period (purple curves; Fig. 5b, e, h, k, and n), similar exponential relationships were observed, and the model fits slightly improved ($R^2$ = 0.71–0.80; *RMSE* = 0.11–1.56 %). For the overall study year (gray curves; Fig. 5c, f, i, l, and o), the relationships were consistent with the seasonal patterns, and the exponential models maintained satisfactory performance ($R^2$ = 0.33–0.80; *RMSE* = 0.11–2.84 %). The fitted exponential parameters revealed distinct differences among canopy vitality stages. The intercept coefficient ($a$), indicating the estimated maximum $S_f$ contribution, ranged from 0.46 to 12.17 across all periods. The highest $a$ values were recorded in healthy trees (Fig. 5a) and top-dry trees (Fig. 5g) during the leaf-on period, whereas the lowest values occurred in branchless snags across all periods (Fig. 5m–o). The exponential rate coefficient ($b$) ranged from 0.11 to 0.83, with higher values generally associated with the snag classes (Fig. 5j–o) and lower values in healthy and fungus-infected trees (Fig. 5a–f). Across all canopy conditions, the exponential models captured the nonlinear increase of $S_f/P_g$ (%) with $P_g$, with maximum $S_f/P_g$ (%) values rarely exceeding 12 %, even during large $P_g$ events.

Exponential models adequately described the relationships between $P_g$ and $I$% across canopy vitality stages and phenological periods (Fig. 6). During the leaf-on period (green curves; Fig. 6a, d, g, j, and m), $I/P_g$ (%) declined rapidly with increasing $P_g$ amount, approaching low asymptotic values beyond approximately 3–8 mm. Model fits were strong, with $R^2$ values ranging from 0.65 to 0.94 and *RMSE* between 1.35 % and 9.36 %. During the leafless period (purple curves; Fig. 6b, e, h, k, and n), $I/P_g$ (%) followed a similar exponential decay pattern, with $R^2$ values of 0.78–0.92 and *RMSE* between 1.64 % and 9.26 %. For the overall study year (gray curves; Fig. 6c, f, i, l, and o), comparable exponential relationships were observed, with model performance ranging from $R^2$ = 0.69–0.85 and *RMSE* = 1.26–13.48 %. The fitted model parameters revealed systematic and consistent variation among canopy vitality stages. The intercept coefficient ($a$), representing the estimated maximum $I/P_g$ (%) at the onset of rainfall amount, ranged from 0.89 to 13.4 across all periods and was generally highest in healthy trees (Fig. 6a–c) and lowest in branchless snags (Fig. 6m–o). The exponential rate coefficient ($b$), indicating the rate of $I/P_g$ (%) decline with $P_g$ amount, varied between –0.44 and –0.51 among canopy vitality stages and periods. The steepest negative $b$ values, reflecting a faster decrease of interception with increasing $P_g$, were found in healthy and fungus-infected trees (Fig. 5a–f), whereas shallower slopes characterized the snag treatments (Fig. 6j–o).

### 3.6. Parametrization of the RGAM

Crown- and trunk-scale ecohydrological parameters exhibited pronounced and systematic variation among canopy vitality stages (Table 4). In both phenological periods, healthy trees consistently maintained the highest values of the inflection point ($I_p$) and crown and trunk storage capacities ($S$ and $S_t$) (Table 4). During the leaf-on period, $I_p$ and $S$ declined from 1.85 mm and 0.78 mm in healthy trees to 0.93 mm and 0.01 mm in branchless snags, respectively, accompanied by a fourfold reduction in the crown saturation threshold ($P'_g$). As canopy vitality decreased, the proportion of free throughfall ($p$) and the ratio of evaporative loss to rainfall ($\bar{E}/\bar{R}$) increased. Trunk-scale parameters followed similar trends: both trunk storage capacity ($S_t$) and the trunk saturation point ($P''_g$) were highest in healthy trees (0.38 mm and 3.22 mm, respectively) and lowest in snags (< 0.01 mm and < 1.1 mm). Across phenological stages, canopy ecohydrological parameters were consistently higher during the leaf-on period than during the leafless period. Despite seasonal reductions in canopy water retention under leafless conditions, the relative ranking among canopy vitality stages remained stable. During the annual period (i.e., overall scale), these vitality-dependent contrasts remained evident (Table 4). Healthy trees exhibited the highest storage capacities ($S$ = 0.55 mm; $S_t$ = 0.31 mm), whereas branchless snags showed minimal values ($S$ = 0.04 mm; $St$ = 0.01 mm) (Table 4). The corresponding saturation thresholds ($P'_g$ and

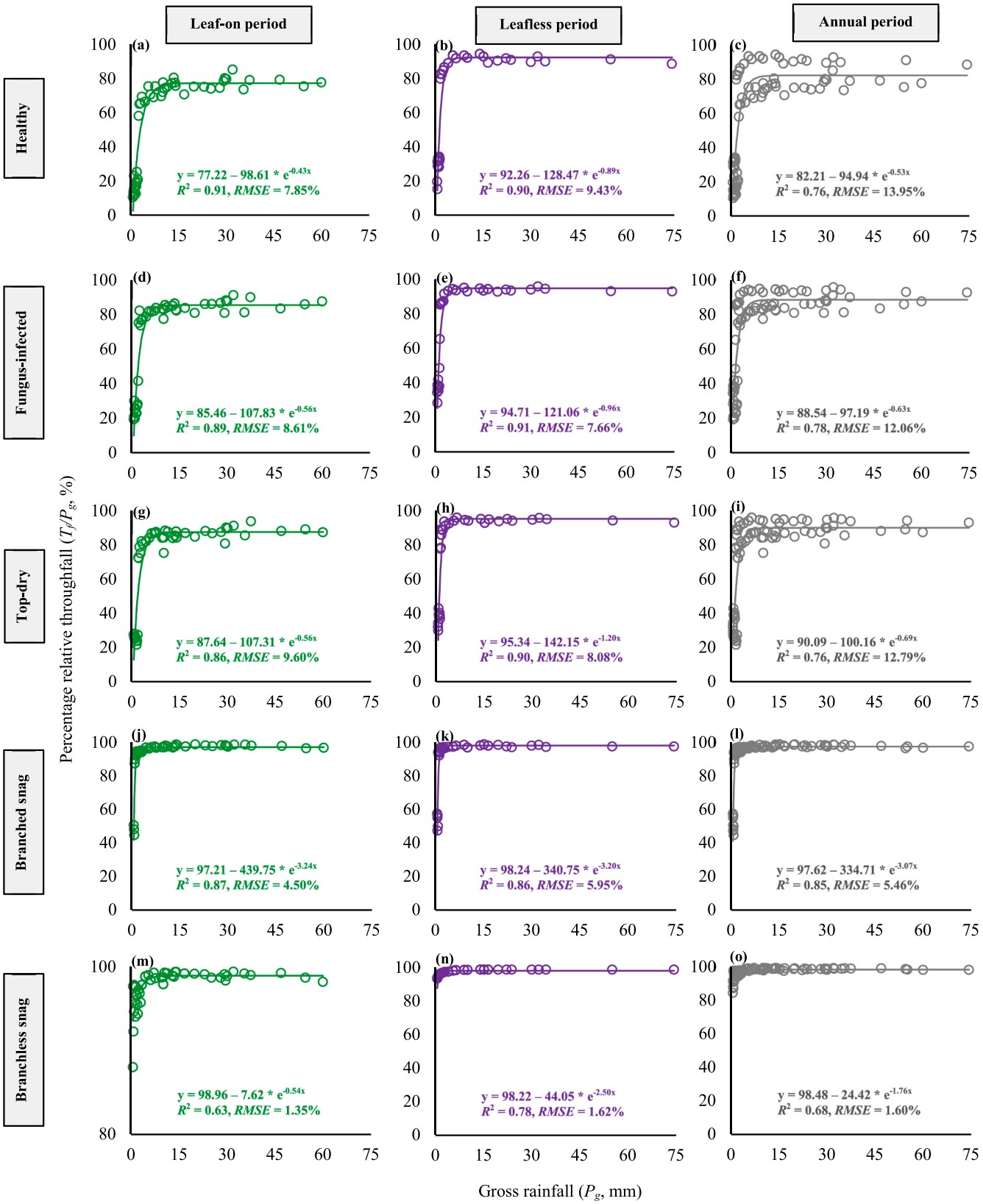



**Fig. 4.** Relationships between gross rainfall ($P_g$) and percentage relative throughfall ($T_f/P_g$ (%)) across five canopy vitality stages during the leaf-on (green), leafless (purple), and annual (dark gray) periods. Panels (a–c) represent healthy trees, (d–f) fungus-infected trees, (g–i) top-dry trees, (j–l) branched snags, and (m–o) branchless snags.

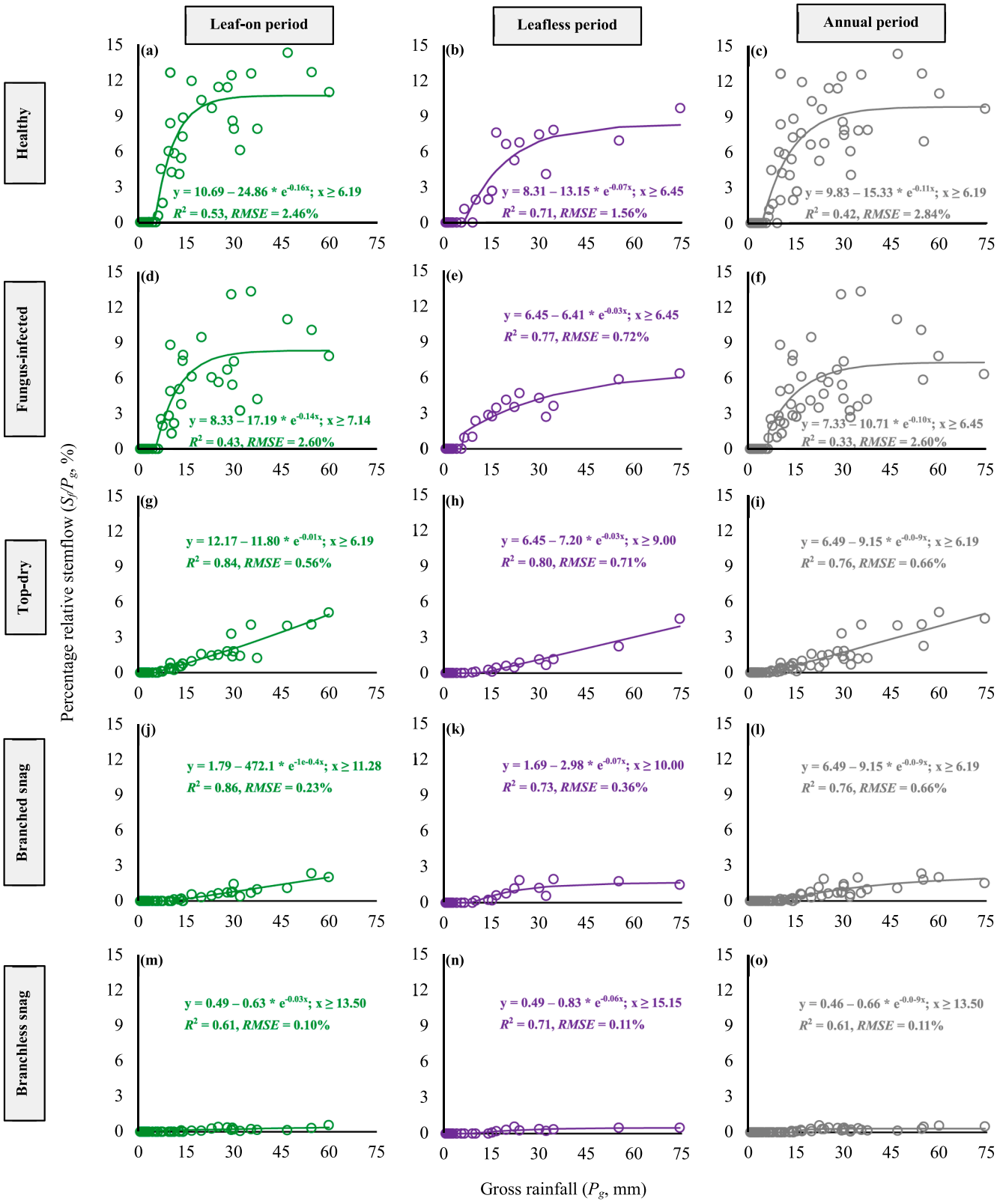



**Fig. 5.** Relationships between gross rainfall ($P_g$) and percentage relative stemflow ($S_f/P_g$ (%)) across five canopy vitality stages during the leaf-on (green), leafless (purple), and annual (dark gray) periods. Panels (a–c) represent healthy trees, (d–f) fungus-infected trees, (g–i) top-dry trees, (j–l) branched snags, and (m–o) branchless snags. The x ≥ values in each panel indicate the $S_f$ generation threshold, i.e., the minimum $P_g$ depth required for measurable $S_f$ initiation.

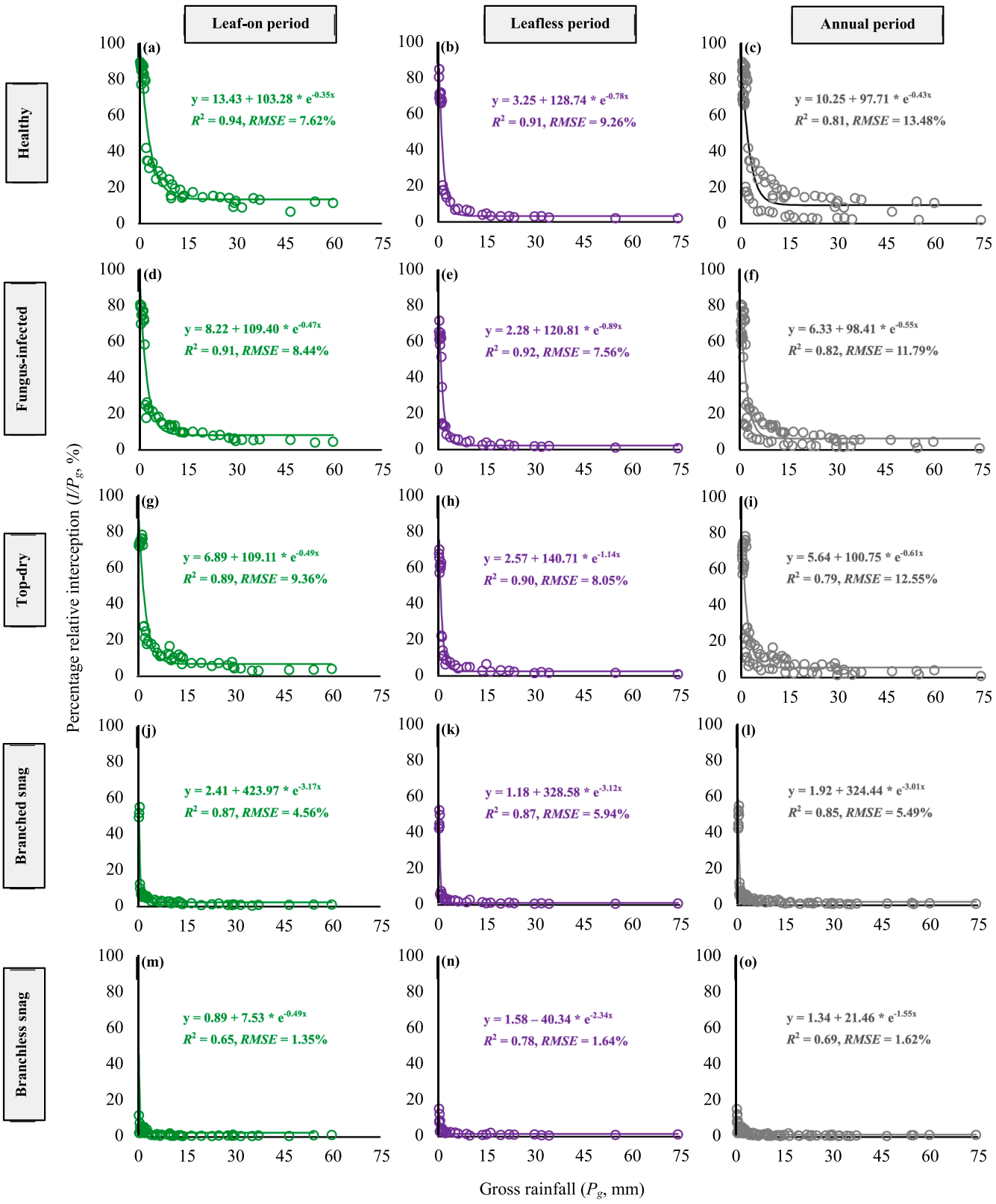



**Fig. 6.** Relationships between gross rainfall ($P_g$) and percentage relative interception ($I/P_g$ (%)) across five canopy vitality stages during the leaf-on (green), leafless (purple), and annual (dark gray) periods. Panels (a–c) represent healthy trees, (d–f) fungus-infected trees, (g–i) top-dry trees, (j–l) branched snags, and (m–o) branchless snags.

**Table 4**
Crown and trunk ecohydrological parameters across five canopy vitality stages of oriental beech trees during the leaf-on, leafless, and annual periods.

| Phenological scale* | Tree vitality stage | Ecohydrological parameters** | | | | | | | |
|---|---|---|---|---|---|---|---|---|---|
| | | Crown | | | | | Trunk | | |
| | | $I_p$ (mm) | $P'_g$ (mm) | $S$ (mm) | $p$ (–) | $\frac{\bar{E}}{\bar{R}}$ (–) | $S_t$ (mm) | $p_t$ (–) | $P''_g$ (mm) |
| Leaf-on | Healthy | 1.85 | 1.05 | 0.78 | 0.18 | 0.21 | 0.38 | 0.11 | 3.22 |
| | Fungus-infected | 1.56 | 0.80 | 0.55 | 0.25 | 0.13 | 0.35 | 0.11 | 3.07 |
| | Top-dry | 1.56 | 0.74 | 0.49 | 0.28 | 0.11 | 0.28 | 0.08 | 3.40 |
| | Branched snag | 0.93 | 0.71 | 0.08 | 0.77 | 0.03 | 0.02 | 0.01 | 2.14 |
| | Branchless snag | 0.93 | 0.25 | 0.01 | 0.95 | 0.01 | 0.001 | 0.002 | 0.3 |
| Leafless | Healthy | 1.66 | 0.72 | 0.17 | 0.69 | 0.11 | 0.30 | 0.08 | 3.53 |
| | Fungus-infected | 1.30 | 0.50 | 0.11 | 0.70 | 0.06 | 0.29 | 0.08 | 3.62 |
| | Top-dry | 1.30 | 0.72 | 0.10 | 0.73 | 0.06 | 0.21 | 0.05 | 4.27 |
| | Branched snag | 0.90 | 0.60 | 0.09 | 0.84 | 0.04 | 0.01 | 0.01 | 1.08 |
| | Branchless snag | 0.80 | 0.23 | 0.02 | 0.97 | 0.02 | 0.002 | 0.003 | 0.68 |
| Annual | Healthy | 1.56 | 1.10 | 0.55 | 0.52 | 0.16 | 0.31 | 0.10 | 3.04 |
| | Fungus-infected | 1.46 | 0.70 | 0.45 | 0.58 | 0.10 | 0.29 | 0.10 | 2.98 |
| | Top-dry | 1.46 | 0.52 | 0.40 | 0.66 | 0.08 | 0.22 | 0.07 | 3.28 |
| | Branched snag | 0.82 | 0.16 | 0.12 | 0.79 | 0.04 | 0.03 | 0.01 | 2.78 |
| | Branchless snag | 0.72 | 0.10 | 0.04 | 0.97 | 0.02 | 0.01 | 0.003 | 1.71 |

* For branched and branchless snags, classification by phenological stage is not ecologically meaningful, as they remain leafless year-round; their values were aligned with the phenological stages of the living trees, which were consistent across all trees.** Abbreviations: $I_p$ – inflection point, $P'_g$ – crown saturation point; $S$ – crown storage capacity; $p$ – free throughfall coefficient; $\bar{E}/\bar{R}$ – ratio of mean evaporation rate from the wet canopy to mean rainfall intensity; $p_t$ – stemflow partitioning coefficient; $S_t$ – trunk storage capacity; $P''_g$ – trunk saturation point.

$P''_g$) were approximately threefold higher in healthy trees than in severely degraded classes (i.e., branchless snag) (Table 4).

### 3.7. Performance of the RGAM

Model performance metrics and the observed–predicted relationships (Fig. 7; Table 5) revealed clear and systematic differences among canopy vitality stages and phenological periods. Across all datasets, the RGAM accurately reproduced canopy interception dynamics for living crowns, as shown by strong 1:1 relationships and regression slopes close to unity (Fig. 6a–f). During the leaf-on period, RGAM showed excellent agreement with observations in healthy and moderately declining trees, with $R^2$ values of 0.93–0.96 and *NSE* values of 0.83–0.95, indicating high predictive reliability. Model skill decreased for top-dry trees ($R^2$ = 0.83, *NSE* = 0.62) and was notably weaker for branched and branchless snags ($R^2$ = 0.65–0.51; *NSE* = 0.41 to –0.29). In the leafless period, the model captured interception reasonably well in living trees ($R^2$ = 0.62–0.76; *NSE* = 0.52–0.68) but performed poorly for snags, particularly branchless ones ($R^2$ = 0.29; *NSE* = –6.05). Regression slopes derived from Fig. 6 further confirmed these trends, with slopes close to 1.0 for healthy and fungus-infected crowns and substantially lower values (< 0.4) for dead canopy classes, reflecting a systematic underestimation of $I$ variability under snag conditions. When data were aggregated across all storm events, RGAM maintained strong predictive performance for healthy and partially declining crowns ($R^2$ = 0.57–0.77; *NSE* = 0.51–0.76), while predictability remained limited for snags ($R^2$ < 0.62; *NSE* < 0.40). Overall, both the statistical performance metrics and the 1:1 relationships demonstrated that model accuracy declined consistently with increasing canopy degradation.

## 4. Discussion

To our knowledge, no previous study has examined rainfall partitioning across such a comprehensive canopy vitality gradient—spanning five distinct stages from healthy trees to completely branchless snags—making direct comparison with earlier research inherently limited. Most previous studies have compared only live versus dead trees or have examined one or two discrete categories of canopy decline (e.g., Hauck et al., 2002; Frost and Levia, 2014; Jeong and Otsuki, 2021; Sadeghi et al., 2023).

### 4.1. Canopy vitality as a driver of rainfall partitioning dynamics

Canopy vitality strongly regulates rainfall partitioning among $T_f$, $S_f$, and $I$, and these relationships scale systematically with $P_g$ amount. As trees transition from healthy to snag stages, the proportion of $P_g$ reaching the forest floor becomes increasingly dominated by $T_f$, while both $I$ and $S_f$ decline sharply (Tables S1–S2). This vitality effect is mechanistically linked to structural changes, such as reduced leaf area (Luo et al., 2024) and branch surface area (Anys and Weiler, 2024), which lower canopy water storage and flow-channeling capacity and shift the canopy from an active hydrological filter toward a more transmissive conduit. Comparable increases in $T_f$ and decreases in $I$ and $S_f$ have been observed following other canopy disturbances that reduce overstory biomass, such as thinning (Ford and Deans, 1978; Hakimi et al., 2018), harvesting (Tomar et al., 2022), heavy ice and snow storms (Wei et al., 2020), pruning (Hakimi et al., 2018), and fire (Brantley et al., 2024). Healthy trees maintained a higher interception capacity, associated with dense foliage and complex branch networks that enhanced rainfall retention and delayed canopy drainage (Kopáček et al., 2020; Sadeghi et al., 2023). In contrast, declining and dead trees exhibited limited rainfall storage, following rapid $T_f$ transmission with minimal modulation of stormwater inputs. Together, these results indicate a $P_g$-dependent shift from buffered to transmissive rainfall delivery as canopy vitality declines, highlighting the central role of canopy structural integrity in regulating forest ecohydrological functioning.

$S_f$ declines track the progressive disconnection of canopy–stem pathways, becoming negligible at the snag stages. Across vitality stages, percentage relative $S_f$ ($S_f/P_g$ (%)) decreased from approximately 3.7 % of $P_g$ in healthy trees to less than 0.1 % in branchless snags (Table S2). This monotonic decline with decreasing canopy vitality reflects a sequential weakening of the interception–funneling continuum that sustains $S_f$ in living crowns. In vigorous trees, intact branch networks and continuous bark flow paths facilitate efficient drainage toward the stem base (Sadeghi et al., 2023; Spittlehouse and Maloney, 2023). As structural deterioration progresses, branch dieback and increased bark roughness disrupt these pathways, reducing the formation, continuity, and stability of water films that channel rainfall to the trunk. Once trees reach the snag stage, $S_f$ almost completely disappears because the loss of branches eliminates the primary initiation points for canopy-to-stem drainage. Importantly, previous studies in the Hyrcanian forest have often neglected $S_f$ contributions in beech stands, assuming them to be

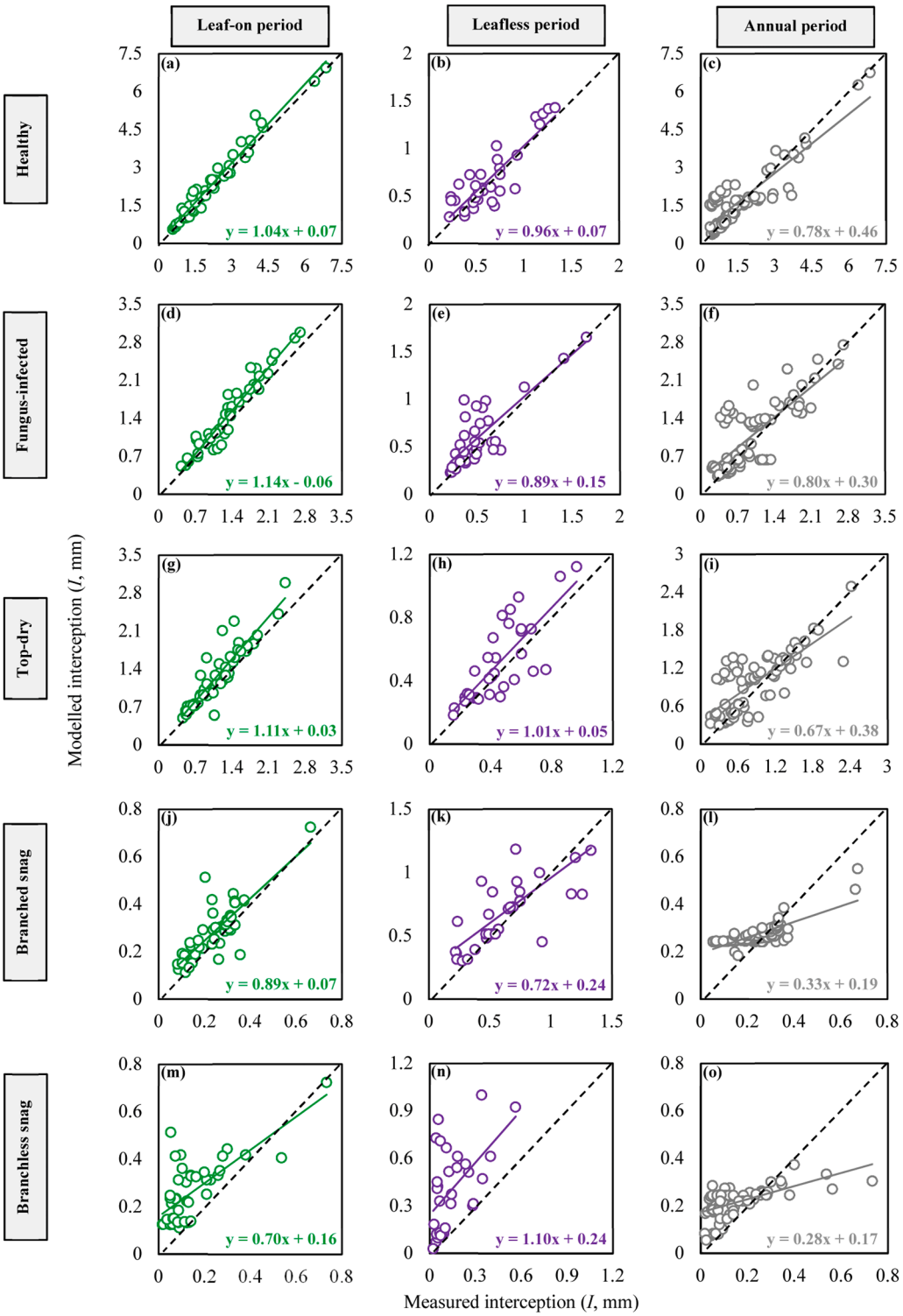



**Fig. 7.** Relationships between observed interception (*I*) and predicted *I* using the reformulated Gash analytical model (RGAM) across five canopy vitality stages during the leaf-on (green), leafless (purple), and annual (dark gray) periods. Panels (a–c) represent healthy trees, (d–f) fungus-infected trees, (g–i) top-dry trees, (j–l) branched snags, and (m–o) branchless snags. The dashed line in each panel indicates the 1:1 line.

negligible (e.g., Abbasian et al., 2015; Moslehi et al., 2019). Our findings directly challenge this assumption by demonstrating that healthy oriental beech trees can generate stemflow equivalent to 3.7 % of $P_g$, corresponding to approximately 11.8 % of cumulative *I* on an annual basis. This near disappearance of $S_f$ in degraded stages thus marks a critical ecohydrological threshold—the loss of localized soil wetting and nutrient transfer that typically occurs around stem bases (Fujimoto et al., 1996). Consistent patterns reported under tree mortality and canopy degradation (Frost and Levia, 2014; Jeong and Otsuki, 2021; Sadeghi et al., 2023; Hauck et al., 2002) further confirm a collapse of stem-directed fluxes with declining canopy vitality. Because $S_f$ act as a focused conduit for water and solutes to the stem-base soil (Katul et al., 2025) and crown structural connectivity progressively declines during tree death and snag formation, the near-complete loss of $S_f$ in snag stages

**Table 5**
Evaluation of canopy interception estimates and model performance statistics derived from the reformulated Gash analytical model (RGAM) across the studied canopy vitality stages during the leaf-on ($n = 45$ storms), leafless ($n = 32$ storms), and annual ($n = 77$ storms) periods.

| Phenological scale* | Tree vitality stage | Mean observed $I$ (mm) | Mean predicted $I$ (mm) | Model performance metric | | |
|---|---|---|---|---|---|---|
| | | | | ***RMSE*** **(mm)** | $R^2$ **(–)** | ***NSE*** **(–)** |
| Leaf-on | Healthy | 2.21 | 2.36 | 0.324 | 0.964 | 0.946 |
| | Fungus-infected | 1.33 | 1.45 | 0.224 | 0.929 | 0.831 |
| | Top-dry | 1.13 | 1.29 | 0.281 | 0.827 | 0.624 |
| | Branched snag | 0.25 | 0.29 | 0.080 | 0.652 | 0.413 |
| | Branchless snag | 0.14 | 0.26 | 0.152 | 0.510 | -0.290 |
| Leafless | Healthy | 0.65 | 0.69 | 0.171 | 0.759 | 0.684 |
| | Fungus-infected | 0.54 | 0.62 | 0.216 | 0.662 | 0.507 |
| | Top-dry | 0.46 | 0.52 | 0.163 | 0.618 | 0.275 |
| | Branched snag | 0.25 | 0.29 | 0.080 | 0.652 | 0.413 |
| | Branchless snag | 0.15 | 0.40 | 0.340 | 0.289 | -6.049 |
| Annual | Healthy | 1.58 | 1.69 | 0.638 | 0.768 | 0.761 |
| | Fungus-infected | 0.97 | 1.08 | 0.404 | 0.617 | 0.532 |
| | Top-dry | 0.85 | 0.96 | 0.349 | 0.571 | 0.510 |
| | Branched snag | 0.23 | 0.27 | 0.094 | 0.613 | 0.361 |
| | Branchless snag | 0.15 | 0.21 | 0.127 | 0.345 | 0.069 |

* For branched and branchless snags, classification by phenological stage is not ecologically meaningful, as they remain leafless year-round; their values were aligned with the phenological stages of the living trees, which were consistent across all trees.

may remove a key pathway for localized moisture and nutrient delivery—potentially impairing microbial activity, nutrient cycling, and regeneration niches in the immediate vicinity of the trunk.

Our results show that canopy vitality systematically simplifies $P_g$ partitioning relationships (Figs. 4–6). For instance, $T_f/P_g$ (%) curves converge toward near-complete rainfall transmission with increasing $P_g$ amount as tree vitality declines (Fig. 4). The partitioning of $P_g$ into $S_f$ decreases from several percent in healthy trees to negligible values in snags (Fig. 5), indicating progressively impaired canopy–stem connectivity. Likewise, $I/P_g$ (%) drops to consistently low values in degraded stages, reflecting reduced canopy storage capacities ($S$ and $S_t$) and a diminished evaporative potential (Fig. 6). Collectively, these patterns demonstrate that declining canopy vitality flattens and linearizes $P_g$ partitioning relationships, with degraded canopies exhibiting uniform, threshold-free responses, in contrast to the nonlinear and highly variable behavior of healthy crowns. Consistent with H1, these contrasts were most pronounced during the leaf-on season, whereas responses converged across canopy vitality stages in the leafless season, when canopy surface area and structural complexity were minimal.

### 4.2. Influence of canopy vitality on ecohydrological parameters

Canopy vitality exerted a strong and mechanistic control over crown-level hydrological parameters that regulate rainfall redistribution. Declining vitality reduced crown storage capacity ($S$) and raised the free-throughfall fraction ($p$), and these patterns matched the observed increase in $T_f$ across vitality decline stages (Fig. 3; Tables S1–S3). Healthy trees, with abundant leaves and fine twigs, retained water for longer durations, prolonging wetting, delaying drainage, and increasing $I$. These results align with earlier work showing that fine crown elements disproportionately sustain canopy buffering and evaporative losses (Pypker et al., 2011; Sadeghi et al., 2023).

Reductions in storage and saturation parameters ($S$, $S_t$, $P'_g$, and $P''_g$) with declining canopy vitality compress the canopy-wetting phase and accelerate the onset of free drainage. In declining trees, $T_f/P_g$ (%)–$P_g$ curves reach their asymptotes at substantially lower $P_g$ values (Fig. 4), indicating a rapid exhaustion of canopy storage capacity. The accompanying flattening of $I/P_g$ (%)–$Pg$ relationships at higher $P_g$ amounts (Fig. 6) reflects a minimal sensitivity of interception to storm size once canopy storage has effectively collapsed. This mechanism is fully consistent with previously documented declines in $S$ and $P'_g$ under crown thinning caused by dieback in oak trees (Sadeghi et al., 2023). The loss of fine foliage and branch surface area accelerates storage depletion, shortens pre-saturation duration, and advances the timing and magnitude of $T_f$ peaks at the forest floor.

Greater canopy openness elevates the free-throughfall fraction ($p$) and increases the proportion of rainfall routed directly to the forest floor. Steeper initial slopes of $T_f/P_g$ (%) vs. $P_g$—especially under leafless conditions (Fig. 4)—indicate higher $p$ values (Table 4), reflecting reduced drip-point density and wider vertical gaps in degraded crowns. The rapid decay of $I/P_g$ (%) observed in Fig. 6, coupled with increases in $p$ reported under canopy-reducing disturbances (Del Campo et al., 2022; Sadeghi et al., 2023), further supports this interpretation: as structural discontinuity increases, the canopy's filtering capacity progressively diminishes.

Wet-canopy evaporation ($\bar{E}/\bar{R}$) plays a progressively diminishing role in rainfall partitioning as canopy vitality declines. In healthy crowns, larger canopy storage capacities, dense leaf–twig networks, and continuous water films extend canopy water residence times and promote evaporative losses, producing the strong curvature in $T_f/P_g$ (%)–$P_g$ relationships and gradual decline of $I/P_g$ (%) with $P_g$ amounts (Figs. 4 and 6; Link et al., 2004; Herbst et al., 2008). With declining canopy vitality, the loss of fine canopy surfaces sharply reduces $S$, $S_t$, and water-film continuity, leading to rapid canopy saturation and an earlier transition to free drainage. These structural changes flatten the $T_f/P_g$ (%)–$P_g$ and $I/P_g$ (%)–$P_g$ relationships, reflecting a minimal evaporative influence once canopy storage is depleted—a pattern consistent with thinned or otherwise disturbed canopies that lose interception capacity (Fathizadeh et al., 2018; Sadeghi et al., 2023). During the leafless season, reduced canopy surface area and short water residence times result in nearly linear $T_f/P_g$ (%)–$P_g$ and $I/P_g$ (%)–$P_g$ relationships across all canopy vitality stages, indicating uniformly low values of $\bar{E}/\bar{R}$. Overall, canopy decline constrains both the duration and effectiveness of wet-canopy evaporation by limiting storage capacity, evporative surface area, and the structural continuity required for sustained evaporative control over rainfall partitioning.

Trunk-level parameters further confirm the progressive weakening of $S_f$ production with declining vitality. The stemflow partitioning coefficient ($p_t$) decreased sharply from healthy trees to snags, and the $P_g$ thresholds required to initiate $S_f$ increased from ~6 mm in healthy crowns to > 13 mm in branchless snags (Table S4). Reduced canopy contact, sparser branching, and disrupted bark continuity require larger storm inputs to overcome surface roughness and establish continuous flow paths (Tonello et al., 2021; Lima et al., 2025; Katul et al., 2025). However, for branched and especially branchless snags, the elevated $P_g$ thresholds required to initiate $S_f$ should be interpreted with caution. Because these trees possess little or no canopy, the canopy–stem transfer pathway is largely absent, and $S_f$ generation is therefore not

mechanistically controlled by bark resistance or surface hardness. Instead, the regression-based estimation of trunk parameters ($S_f$ vs. $P_g$) implies that detectable $S_f$ in snags occurs only during very large rainfall events, likely reflecting incidental bole wetting or limited direct routing along the trunk. Consequently, this apparent threshold represents a functional loss of canopy-mediated water concentration rather than an increase in trunk surface resistance. Elevated thresholds and reduced $p_t$ therefore indicate the near disappearance of true canopy-derived $S_f$ and demonstrate a fundamental breakdown of $S_f$-collection efficiency, with major implications for near-stem water and nutrient delivery under declining canopy vitality.

### 4.3. Phenoseasonal contrasts in rainfall partitioning and canopy ecohydrological parameters

Phenoseasonal canopy dynamics exerted a strong and systematic control on rainfall partitioning across all canopy vitality stages. During the leaf-on period, $I$ and $S_f$ were consistently higher, while $T_f$ was lower and more variable, reflecting the role of active foliage and fine twigs in storing and redistributing rainfall. In contrast, during the leafless period, $T_f$ increased sharply, and both $I$ and $S_f$ declined, producing nearly linear $T_f/P_g$ (%)–$P_g$ and $I/P_g$ (%)–$P_g$ relationships (Figs. 4–6). These changes correspond to the loss of foliage and the reduction in effective canopy surface area available for temporary water storage and funneling (Sadeghi et al., 2020). The magnitude of seasonal contrasts was greatest in healthy and moderately declined trees, where foliage presence amplified storage capacity and drainage heterogeneity, but progressively diminished with canopy degradation. In snag stages, rainfall redistribution showed little to no seasonal variation, because the structural elements responsible for phenological effects were largely absent. This pattern indicates that phenoseasonal variability is most relevant in living crowns with intact leaf area and declines sharply once canopy mortality advances (Herbst et al., 2008; Fathizadeh et al., 2018; Sadeghi et al., 2023).

Seasonal canopy conditions also influenced key ecohydrological parameters that mechanistically regulate rainfall partitioning. $S$ and $P'_g$ were substantially higher during the leaf-on season, whereas the $p$ increased in the leafless season as a larger proportion of rainfall bypassed the canopy directly (Table 4). Similarly, the wet-canopy evaporation ratio ($\bar{E}/\bar{R}$) exerted stronger control over rainfall losses in the leaf-on season, when retained water could evaporate over longer residence times. These differences confirm that the canopy's hydrological buffering capacity is strongly season-dependent and largely controlled by the presence of foliage and fine crown element s(Herbst et al., 2008; Sadeghi et al., 2015; Sadeghi et al., 2018). However, the seasonal contrast in $S$, $p$, and $\bar{E}/\bar{R}$ weakened with declining vitality, consistent with structural simplification, reduced surface area, and the loss of active hydrological interfaces in degraded crowns. Overall, the interaction between canopy vitality and phenoseason defines the temporal limits of rainfall regulation, with strong seasonal modulation in healthy, foliated crowns, and nearly absent in dead or severely degraded trees, where canopy structure no longer supports meaningful hydrological buffering.

### 4.4. Modeling performance of RGAM to estimate interception

Recent critiques highlight that hydrological models often universalize empirical relationships originating from a narrow set of historical and geographical contexts, which can reproduce epistemic dominance by embedding place-specific assumptions as global truths (Van Stan and Simmons, 2025). In $I$ modeling, this tendency is especially visible: parameters derived from temperate British forests (Gash et al., 1995) or controlled conifer experiments in North America (Lundquist et al., 2021) have been abstracted into global routines that overlook canopy structures, climates, and ecohydrological processes that diverge sharply from their empirical roots. Our results provide a concrete and process-based example of this limitation, showing both where such inherited formulations remain robust and where they fail under the distinct structural complexity and canopy vitality gradients characteristic of old-growth Hyrcanian oriental beech stands.

The RGAM accurately captured interception dynamics across canopy vitality stages but exhibited systematic variation in performance depending on crown condition and phenoseason. Healthy and moderately degraded trees showed the strongest agreement between observed and predicted $I$, confirming that RGAM effectively represents rainfall–storage processes in structurally intact and partially functional canopies. In contrast, predictive accuracy declined markedly for snags. These discrepancies arise because RGAM implicitly assumes continuous canopy coverage and relatively homogeneous storage capacity, assumptions that break down once foliage and branches are lost and canopy structure becomes fragmented.

Model performance differed notably between phenoseasons, reflecting the changing canopy structure and water storage capacity. During the leaf-on period, RGAM reproduced observed $I$ well for healthy and partially degraded trees, because leaf surfaces and fine branches supported sufficient storage and evaporation surface area for the model assumptions to remain valid. In contrast, during the leafless period, the model systematically overestimated $I$ across all vitality classes, as the simplified canopy structure reduced both $S$ and $\bar{E}/\bar{R}$ beyond what is represnted in the model parameterization. This seasonal divergence indicates that RGAM's static representations of storage and evaporation parameters cannot fully capture the temporal variability of canopy hydrological functioning, especially in ecosystems with pronounced phenological dynamics. Similar performance declines under defoliated, thinned, or structurally simplified canopies have been reported in other applications of the Gash framework (Mużyło et al., 2012; Fathizadeh et al., 2018; Andreasen et al., 2023), reinforcing the need for phenology-sensitive parameterization in $I$ modeling.

Vitality-related deviations between modeled and observed $I$ further show the strong dependence of RGAM on canopy structural integrity. As vitality decreased, the model consistently underestimated the rate at which $I$ declined with $P_g$, producing overly gradual curves relative to measured data. This outcome suggests that assuming constant canopy ecohydrological parameters at the stand or watershed scale may not be realistic, particularly in structurally heterogeneous forests. Incorporating variable storage terms, crown porosity indices (Van Stan et al., 2016; Sadeghi et al., 2024), or vitality-dependent parameterization could improve the performance of RGAM. However, applying such refinements can be challenging in practice, since quantifying structural heterogeneity and vitality composition across stands requires detailed field data. Moreover, the strong linearity of observed $I$–$P_g$ relationships in branchless snags (Figs. 6m to 6o) implies that simplified empirical formulations may outperform physically based models when canopy retention is minimal. Overall, RGAM proved robust for estimating $I$ in healthy and moderately degraded trees, but became unreliable under severe canopy decline conditions. The model's structural assumptions—uniform canopy coverage, constant storage capacity, and fixed evaporation ratios—limit its applicability in stands with high structural heterogeneity, extensive canopy gaps, or large proportions of snags. Therefore, while RGAM remains effective for intact or moderately disturbed forests, caution is needed when applying it to mixed-vitality or open-canopy systems where its simplifying assumptions are violated.

These findings reinforce the broader argument that hydrological models built from geographically limited empirical foundations risk "flattening" hydrological realities when applied in ecosystems with contrasting canopy structures, climate regimes, or disturbance histories (Van Stan and Simmons, 2025). By empirically demonstrating how $I$ behavior transforms across a five-stage canopy vitality gradient, our study provides the type of place-based evidence needed to counter abstraction-driven biases and to guide more realistic, structure-sensitive parameterization of $I$ processes in structurally diverse forests. Our results therefore argue for a shift from treating canopy structure as

background variability to recognizing it as a core organizing principle of ecohydrological modeling. Place-based evidence does not weaken general theory; it anchors theory in the diversity of real landscapes. Only by embracing structural and ecological specificity can $I$ modeling move beyond abstraction and toward a more faithful representation of how forests actually mediate water, energy, and matter.

### 4.5. Management implications

The progressive decline in canopy vitality transforms forest canopies from hydrologically buffering systems into more transmissive, homogeneous rainfall filters, with direct consequences for forest water regulation and soil processes. The combined reduction in $I$ and $S_f$, together with increased $T_f$, indicates a structural simplification of rainfall redistribution pathways as trees deteriorate. Healthy, structurally complex canopies promote rainfall retention and spatial heterogeneity in soil wetting, whereas degraded or dead trees produce more uniform but hydrologically less diverse rainfall inputs. This homogenization can diminish near-stem soil moisture gradients (Frost and Levia, 2014), alter microbial and root activity (Mohammadrad et al., 2020), and reduce the ecological distinctiveness of microsites. From a management perspective, maintaining stands with a diversity of vitality stages and structural complexity is essential to sustain canopy water-partitioning regulation and soil hydrological variability. Furthermore, vitality-driven changes in rainfall partitioning interact with reductions in transpiration to influence stand-scale evapotranspiration and water yield, emphasizing the need to explicitly incorporate canopy vitality dynamics into hydrological modeling (Bai et al., 2018), forest health monitoring (Safe'i et al., 2022), and adaptive management planning (Fuller and Quine, 2016).

Management practices in Iran provide a clear example of how evolving silvicultural philosophies can influence forest hydrology. Historically, under the classical forestry approach, managers routinely removed deadwood and declining trees to maintain "forest health" and maximize timber productivity (Marvie Mohadjer, 2011). Since the introduction of "close-to-nature silviculture" in the 1990s, however, management policy has shifted toward retaining deadwood and trees with reduced vitality as essential microhabitat elements that enhance stand biodiversity and resilience (Marvie Mohadjer, 2011; Sagheb Talebi, 2017). Our results show that this shift also has direct hydrological consequences and should be interpreted as a water-regulation strategy, not solely a biodiversity-driven decision. Despite this shift, the hydrological consequences of such retention practices have rarely been examined. Many hydrological models still assume that snags—whether branched or branchless—have negligible interception capacity (Tague and Band, 2004). Yet, existing studies indicate that incorporating deadwood elements improves model realism and water-balance predictions (Ren et al., 2021). Our findings further demonstrate that this assumption is inaccurate: even at the annual scale, percentage relative interception ($I/P_g$ (%)) reached 7.9 % in branched snags and 2.8 % in branchless snags. Therefore, completely excluding these canopy components from water balance calculations can lead to systematic underestimation of interception losses and overestimation of net precipitation reaching the forest floor. From a silvicultural perspective, this means that the retention of declining trees and snags modifies not only habitat structure but also the spatial and quantitative distribution of water inputs to the soil. Integrating realistic interception contributions from declining and dead trees into hydrological modeling would enhance predictions of soil moisture, recharge, and stand-level water cycling in mixed-vitality forests.

Canopy ecohydrological parameters also provide measurable indicators for assessing canopy health and hydrological function under progressive decline. By quantifying storage and flow characteristics across a five-stage vitality gradient, this study demonstrates that even early and visually subtle stages of canopy degradation can substantially alter rainfall–canopy interactions and water redistribution pathways. The observed parameter shifts reflect a loss of canopy water-regulation capacity and can therefore serve as sensitive indicators of hydrological dysfunction in declining forests. Long-term monitoring of these ecohydrological parameters would allow forest managers to detect early structural deterioration before major canopy collapse occurs, support timely and targeted interventions, and maintain forest water balance through adaptive management. Integrating such ecohydrological metrics into forest health assessments can also help predict shifts in evapotranspiration, infiltration, and soil moisture distribution, thereby improving the capacity of forest management strategies to sustain ecosystem resilience under ongoing disturbance pressure and climate stress. A brief overview of study limitations and future research needs is provided in the Supplementary Material.

## 5. Conclusions

The ecohydrological consequences of tree vitality decline remain poorly understood. This one-year study in an old-growth Hyrcanian oriental beech (*F. orientalis*) forest confirmed that canopy vitality strongly regulates rainfall partitioning, consistent with our first hypothesis (H1). Rainfall redistribution differed markedly between the leaf-on and leafless seasons, with pronounced contrasts among vitality classes during the leaf-on period when canopy surfaces were hydrologically active. As predicted by H2, degraded trees exhibited distinct and simplified rainfall-partitioning patterns, as stemflow decreased sharply with declining vitality and was consistently lower during the leafless period, reflecting the fundamental dependence of trunk water fluxes on canopy structural integrity and phenoseasons.

Even snag trees retained a measurable hydrological function, intercepting roughly 5 % of annual rainfall—an amount that should be explicitly considered in forest water-balance models. Ignoring this contribution would lead to a systematic underestimation of interception and a corresponding overestimation of effective precipitation reaching the forest floor. In line with H3, the RGAM successfully simulated interception in healthy and moderately degraded crowns, but performed less reliably in severely deteriorated or snag canopies. These results indicate that RGAM parameters must be recalibrated to account for structural decline, or alternatively, that simpler linear or emprical formulations may be more appropriate when canopy storage and evaporation capacity are minimal.

Overall, acknowledging the residual hydrological role of dead and declining trees—and adjusting hydrological models accordingly—will substantially improve predictions of rainfall redistribution, soil moisture dynamics, and water yield in mixed-vitality stands of the Hyrcanian forest, and by extension, in old-growth temperate forests worldwide.

## CRediT authorship contribution statement

**Seyed Mohammad Moein Sadeghi:** Writing – review & editing, Writing – original draft, Visualization, Supervision, Software, Methodology, Formal analysis, Data curation, Conceptualization. **Hamed Aghajani:** Writing – review & editing, Project administration, Investigation, Funding acquisition. **Hamid Jalilvand:** Writing – review & editing. **Salman Ahmady-Asbchin:** Writing – review & editing. **Seyed Mazyar Sadati:** Writing – review & editing. **Miriam Coenders-Gerrits:** Writing – review & editing. **Salli F. Dymond:** Writing – review & editing, Formal analysis.

## Supplemental material

Word file containing supplementary information are provided as supplementary material.

## Funding

Funding to support Hamed Aghajani, Hamid Jalilvand, Salman Ahmady-Asbchin, and Seyed Mazyar Sadati was provided by the Sari

Agricultural Sciences and Natural Resources University under project number 04–1403–08. Seyed Mohammad Moein Sadeghi, Miriam Coenders-Gerrits, and Salli F. Dymond received no specific funding for this work. The authors gratefully acknowledge the efforts and collaboration of the Sari Agricultural Sciences and Natural Resources University for supporting the approved research project entitled *"Molecular identification of micromycete (hyphomycete) fungi and bacteria associated with stemflow and throughfall in Fagus orientalis within Darabkola Forest."*

## Declaration of Competing Interest

The authors declare that they have no known competing financial interests or personal relationships that could have appeared to influence the work reported in this paper.

## Acknowledgment

We gratefully thank the staff of Darabkola Forest for their valuable assistance in maintaining the instruments and supporting field data collection.

## Appendix A. Supporting information

Supplementary data associated with this article can be found in the online version at doi:10.1016/j.foreco.2026.123552.

## Data Availability

Data will be made available on request.

## References

Abbasian, P., Attarod, P., Sadeghi, S.M.M., Van Stan, J.T., Hojjati, S.M., 2015. Throughfall nutrients in a degraded indigenous *Fagus orientalis* forest and a *Picea abies* plantation in the of North of Iran. For. Syst. 24 (3), e035.

Abdi, E., Samdaliry, H., Ghalandarayeshi, S.H., Khoramizadeh, A., Sohrabi, H., Deljouei, A., Kvist Johannsen, V., Etemad, V., 2020. Modeling wind-driven tree mortality: the effects of forest roads. Austrian J. For. Sci. 137, 1–21.

Aghajani, H., Marvie Mohadjer, M.R., Bari, E., Ohno, K.M., Shirvany, A., Asef, M.R., 2018. Assessing the biodiversity of wood decay fungi in northern forests of Iran. Proc. Natl. Acad. Sci. India Sect. B Biol. Sci. 88 (4), 1463–1469.

Alavi, S.J., Veiskarami, R., Esmailzadeh, O., Gadow, K.V., 2020. Analyzing the biological and structural diversity of Hyrcanian forests dominated by *Taxus baccata* L. Forests 11 (6), 701.

Allen, R.G., Pereira, L.S., Raes, D., Smith, M., 1998. Crop evapotranspiration-Guidelines for computing crop water requirements-FAO Irrigation and drainage paper 56, 300. FAO, *Rome*.

Andreasen, M., Christiansen, J.R., Sonnenborg, T.O., Stisen, S., Looms, M.C., 2023. Seasonal dynamics of canopy interception loss within a deciduous and a coniferous forest. Hydrol. Process. 37 (4), e14828.

Anonymous. (2008). Management Plan of the Darabkola Forest. Forest, Range and Watershed Management Organization, Sari, Iran, 210 p (In Persian).

Anys, M., Weiler, M., 2024. Rainfall interception by urban trees: event characteristics and tree morphological traits. Hydrol. Process. 38 (4), e15146.

Azaryan, M., Abrari Vajari, K., Marcu, M.V., Sadeghi, S.M.M., 2025. Integrating multiscale ecological indicators to assess ecosystem functioning in virgin Hyrcanian beech forests. Front. For. Glob. Change 8, 1726336.

Bai, P., Liu, X., Zhang, Y., Liu, C., 2018. Incorporating vegetation dynamics noticeably improved performance of hydrological model under vegetation greening. Sci. Total Environ. 643, 610–622.

Brantley, S.T., Stuber, O.S., Holder, D.L., Taylor, R.S., 2024. Fire exclusion alters forest evapotranspiration: a comprehensive water budget analysis in longleaf pine woodlands. Ecol. Monogr. 94 (4), e1623.

Chen, J., Shao, C., Jiang, S., Qu, L., Zhao, F., Dong, G., 2019. Effects of changes in precipitation on energy and water balance in a Eurasian meadow steppe. Ecol. Process. 8 (1), 17.

Coenders-Gerrits, M., Schilperoort, B., Jiménez-Rodríguez, C., 2020. Evaporative processes on vegetation: an inside look. Precipitation partitioning by vegetation: A global synthesis. Springer International Publishing, Cham, pp. 35–48.

Del Campo, A.D., Otsuki, K., Serengil, Y., Blanco, J.A., Yousefpour, R., Wei, X., 2022. A global synthesis on the effects of thinning on hydrological processes: implications for forest management. For. Ecol. Manag. 519, 120324.

Dietz, J., Hölscher, D., Leuschner, C., 2006. Rainfall partitioning in relation to forest structure in differently managed montane forest stands in Central Sulawesi, Indonesia. For. Ecol. Manag. 237 (1-3), 170–178.

Etemad, S.S., Mohammadi Limaei, S., Yousefpour, R., 2025. Simulating the effects of climate change on the growth and management of uneven-aged Oriental beech (*Fagus orientalis* L.) in Hyrcanian forests of Iran. Eur. J. For. Res. 1–17.

Farashiani, M.E., Ahmadi, S.M., Zarghani, E., Kazerani, F., Naji, H.R., 2023. Study of some biological properties of Xylophagous beetle, *Morimus verecundus* in laboratorial and field conditions. Iran. J. For. Range Prot. Res. 21 (2), 240–252.

Fathizadeh, O., Hosseini, S.M., Keim, R.F., Boloorani, A.D., 2018. A seasonal evaluation of the reformulated Gash interception model for semi-arid deciduous oak forest stands. For. Ecol. Manag. 409, 601–613.

Fischer-Bedtke, C., Metzger, J.C., Demir, G., Wutzler, T., Hildebrandt, A., 2023. Through Spat. Patterns Transl. into Spat. Patterns Soil moisture Dyn. Empir. Evid. Hydrol. Earth Syst. Sci. 27 (15), 2899–2918.

Ford, E.D., Deans, J.D., 1978. The effects of canopy structure on stemflow, throughfall and interception loss in a young Sitka spruce plantation. J. Appl. Ecol. 905–917.

Frost, E.E., Levia Jr, D.F., 2014. Hydrologic variation of stemflow yield across co-occurring dominant canopy trees of varying mortality. Ecohydrology 7 (2), 760–770.

Fujimoto, K., Sakai, Y., Nishimura, T., Arimitsu, K., 1996. Influence of stemflow of dead Japanese red pine (*Pinus densflora* Sieb. et Zucc.) on soil properties. Jpn. J. For. Environ. 38, 98–108.

Fuller, L., Quine, C.P., 2016. Resilience and tree health: a basis for implementation in sustainable forest management. For. Int. J. For. Res. 89 (1), 7–19.

Gash, J.H., Lloyd, C.R., Lachaud, G., 1995. Estimating sparse forest rainfall interception with an analytical model. J. Hydrol. 170 (1-4), 79–86.

Gash, J.H.C., Morton, A.J., 1978. An application of the Rutter model to the estimation of the interception loss from Thetford forest. J. Hydrol. 38 (1-2), 49–58.

Grundmann, M.H., Molnar, P., Floriancic, M.G., 2024. Quantification of enrichment processes in throughfall and stemflow in a mixed temperate forest. Hydrol. Process. 38 (7), e15224.

Hakimi, L., Sadeghi, S.M.M., Van Stan, J.T., Pypker, T.G., Khosropour, E., 2018. Management of pomegranate (*Punica granatum*) orchards alters the supply and pathway of rain water reaching soils in an arid agricultural landscape. Agric. Ecosyst. Environ. 259, 77–85.

Hauck, M., Hesse, V., Runge, M., 2002. The significance of stemflow chemistry for epiphytic lichen diversity in a dieback-affected spruce forest on Mt Brocken, northern Germany. Lichenologist 34 (5), 415–427.

Herbst, M., Rosier, P.T., McNeil, D.D., Harding, R.J., Gowing, D.J., 2008. Seasonal variability of interception evaporation from the canopy of a mixed deciduous forest. Agric. For. Meteorol. 148 (11), 1655–1667.

Jahdi, R., Nejad, A.S., Behjou, F.K., 2023. Assessing the state of forest health in Oriental beech (*Fagus orientalis* L.) dominated forests in Iran. Ann. Silvic. Res. 48 (2), 60–72.

Jeong, S., Otsuki, K., 2021. Effects of tree mortality on the estimation of stemflow yield in a self-thinning coniferous plantation. Ecohydrology 14 (7), e2327.

Jeong, S., Nanko, K., Katayama, A., Kume, T., Koga, S., Otsuki, K., 2024. Characteristics of throughfall kinetic energy in an unmanaged Japanese cypress plantation laden with dead branches. Catena 243, 108181.

Jörg, M., Simon, T., Roland, B., Sagheb-Talebi, K., Barimani, H.V., Sebastian, S., Ulyshen, M.D., Gossner, M.M., 2016. Protecting the forests while allowing removal of damaged trees may imperil saproxylic insect biodiversity in the Hyrcanian beech forests of Iran. Conserv. Lett. 9 (2), 106–113.

Katul, G.G., Keshavarz, B., Meydani, A., Levia, D.F., 2025. Stemflow hydrodynamics. Rev. Geophys. 63 (3), e2024RG000857.

Keybondori, S., Abdi, E., Deljouei, A., Cislaghi, A., Shakeri, Z., Etemad, V., 2025. Soil-bioengineering to stabilize gravel roadside slopes in the steep Hyrcanian Forests of Northern Iran. Ecol. Eng. 214, 107569.

Kohler, M., Gorges, J., Andermahr, D., Koelz, A., Leder, B., Nagel, R.V., Mettendorf, B., Le Thiec, D., Skiadaresis, G., Kurz, M., Sperisen, C., Seifert, T., Csilléry, K., Bauhus, J., 2024. A direct comparison of the radial growth response to drought of European and Oriental beech. For. Ecol. Manag. 572, 122130.

Kooch, Y., Nouraei, A., Wirth, S., 2023. Deadwoods are hotspots for soil functions in old-growth beech forests: monitoring during 15 years after a windthrow event. Eur. J. For. Res. 142 (6), 1401–1421.

Kopáček, J., Bače, R., Hejzlar, J., Kaňa, J., Kučera, T., Matějka, K., Porcal, P., Turek, J., 2020. Changes in microclimate and hydrology in an unmanaged mountain forest catchment after insect-induced tree dieback. Sci. Total Environ. 720, 137518.

Král, K., Vrška, T., Hort, L., Adam, D., Šamonil, P., 2010. Developmental phases in a temperate natural spruce-fir-beech forest: determination by a supervised classification method. Eur. J. For. Res. 129 (3), 339–351.

Levia, D.F., Germer, S., 2015. A review of stemflow generation dynamics and stemflow-environment interactions in forests and shrublands. Rev. Geophys. 53 (3), 673–714.

Levia, D.F., Hudson, S.A., Llorens, P., Nanko, K., 2017. Throughfall drop size distributions: a review and prospectus for future research. Wiley Interdiscip. Rev. Water 4 (4), e1225.

Lian, X., Zhao, W., Gentine, P., 2022. Recent global decline in rainfall interception loss due to altered rainfall regimes. Nat. Commun. 13 (1), 7642.

Lima, M.T., Bramorski, J., Tonello, K.C., 2025. Reimagining urban stemflow: How tree traits shape rainfall redistribution in peri-urban environments. Environ. Manag. 75, 3658–3672.

Link, T.E., Unsworth, M., Marks, D., 2004. The dynamics of rainfall interception by a seasonal temperate rainforest. Agric. For. Meteorol. 124 (3-4), 171–191.

Lloyd, C.R., 1990. The temporal distribution of Amazonian rainfall and its implications for forest interception. Q. J. R. Meteorol. Soc. 116 (496), 1487–1494.

Lundquist, J.D., Dickerson-Lange, S., Gutmann, E., Jonas, T., Lumbrazo, C., Reynolds, D., 2021. Snow interception modelling: isolated observations have led to many land surface models lacking appropriate temperature sensitivities. Hydrol. Process. 35 (7), e14274.

Luo, Y., Yang, Q., Zhou, J., Jian, C., Chen, Z., Xiong, P., Palta, J.A., Xu, B., 2024. Aboveground biomass determines canopy rainfall interception loss in Semiarid Grassland Communities. Ecohydrology 17 (6), e2677.
Ma, M., Li, Q., Wang, Y., Liang, J., Wang, J., Liu, J., Zhang, M., 2025. Rainfall intensities determine accuracy of canopy interception simulation using the Revised Gash model. Agric. For. Meteorol. 362, 110389.
Marvie Mohadjer, M.R., 2011. Silviculture, 387. University of Tehran Press, Tehran, Iran.
Maurer, K.D., Hardiman, B.S., Vogel, C.S., Bohrer, G., 2013. Canopy-structure effects on surface roughness parameters: observations in a great lakes mixed-deciduous forest. Agric. For. Meteorol. 177, 24–34.
Mazza, G., Amorini, E., Cutini, A., Manetti, M.C., 2011. The influence of thinning on rainfall interception by *Pinus pinea* L. in Mediterranean coastal stands (Castel Fusano—Rome). Ann. For. Sci. 68 (8), 1323–1332.
McGee, G.G., Cardon, M.E., Kiernan, D.H., 2019. Variation in *Acer saccharum* Marshall (sugar maple) bark and stemflow characteristics: implications for epiphytic bryophyte communities. Northeast. Nat. 26 (1), 214–235.
Mellert, K.H., Šeho, M., 2022. Suitability of *Fagus orientalis* Lipsky at marginal *Fagus sylvatica* L. forest sites in Southern Germany. IForest 15 (5), 417.
Melo Neto, J.O., Rodrigues, A.F., Mello, C.R., 2024. On canopy rainfall interception modeling in a eucalyptus plantation. Forests 15 (9), 1577.
Miralles, D.G., Vilà-Guerau de Arellano, J., McVicar, T.R., Mahecha, M.D., 2025. Vegetation–climate feedbacks across scales. Ann. New Y. Acad. Sci. 1544 (1), 27–41.
Mitsudera, M., Kamata, Y., Nakane, K., 1984. Effect of fire on water and major nutrient budgets in forest ecosystems: III. Rainfall interception by forest canopy. Jpn. J. Ecol. 34 (1), 15–25.
Mohammadrad, A., Abdi, E., PourHashemi, M., Majnounian, B., Deljouei, A., 2020. Effect of oak decline phenomenon on root mechanical characteristics of Brants oak (*Quercus brantii* Lindl.). Iran. J. For. 12 (2), 219–231.
Moslehi, M., Habashi, H., Khormali, F., Ahmadi, A., Brunner, I., Zimmermann, S., 2019. Base cation dynamics in rainfall, throughfall, litterflow and soil solution under Oriental beech (*Fagus orientalis* Lipsky) trees in northern Iran. Ann. For. Sci. 76 (2), 55.
Muzylo, A., Llorens, P., Valente, F., Keizer, J.J., Domingo, F., Gash, J.H.C., 2009. A review of rainfall interception modelling. J. Hydrol. 350 191–206.
Mużyło, A., Valente, F., Domingo, F., Llorens, P., 2012. Modelling rainfall partitioning with sparse Gash and Rutter models in a downy oak stand in leafed and leafless periods. Hydrol. Process. 26 (21), 3161–3173.
Nash, J.E., Sutcliffe, J.V., 1970. River flow forecasting through conceptual models: part 1. A discussion of principles. J. Hydrol. 10, 282–290.
Nazari, M., Sadeghi, S.M.M., Van Stan II, J.T., Chaichi, M.R., 2020. Rainfall interception and redistribution by maize farmland in central Iran. J. Hydrol. Reg. Stud. 27, 100656.
Nezamdoost, H., Sefidi, K., Rasoulzadeh, A., Sadeghi, S.M.M., 2018. Quantifying throughfall, stemflow, and rainfall interception in a *Fagus orientalis* forest and a *Picea abies* plantation in Siahkal, Gilan. Iran. J. For. 9 (3), 385–396.
Owens, M.K., Lyons, R.K., Alejandro, C.L., 2006. Rainfall partitioning within semiarid juniper communities: effects of event size and canopy cover. Hydrol. Process. 20 (15), 3179–3189.
Panahandeh, T., Attarod, P., Sadeghi, S.M.M., Bayramzadeh, V., Tang, Q., Liu, X., 2022. The performance of the reformulated Gash rainfall interception model in the Hyrcanian temperate forests of northern Iran. J. Hydrol. 612, 128092.
Pypker, T.G., Bond, B.J., Link, T.E., Marks, D., Unsworth, M.H., 2005. The importance of canopy structure in controlling the interception loss of rainfall: Examples from a young and an old-growth Douglas-fir forest. Agric. For. Meteorol. 130 (1-2), 113–129.
Pypker, T.G., Levia, D.F., Staelens, J., Van Stan, J.T., 2011. Canopy structure in relation to hydrological and biogeochemical fluxes. Forest Hydrology and Biogeochemistry: Synthesis of Past Research and Future Directions. Dordrecht: Springer, Netherlands, pp. 371–388.
Raziei, T., 2022. Climate of Iran according to Köppen-Geiger, Feddema, and UNEP climate classifications. Theor. Appl. Climatol. 148, 1395–1416.
Ren, J., Adam, J.C., Hicke, J.A., Hanan, E.J., Tague, C.L., Liu, M., Kolden, C.A., Abatzoglou, J.T., 2021. How does water yield respond to mountain pine beetle infestation in a semiarid forest? Hydrol. Earth Syst. Sci. 25 (9), 4681–4699.
Ritz, C., Streibig, J.C., 2005. Bioassay analysis using R. J. Stat. Softw. 12, 1–22.
Roberts, J.M., 2009. The role of forests in the hydrological cycle. Water Interact. Energy Environ. Food Agric. II, 114.
Rodrigues, A.F., de Mello, C.R., Nehren, U., de Coimbra Ribeiro, J.P., Mantovani, V.A., de Mello, J.M., 2021. Modeling canopy interception under drought conditions: The relevance of evaporation and extra sources of energy. J. Environ. Manag. 292, 112710.
Sadeghi, S.M.M., Attarod, P., Pypker, T.G., 2015. Differences in rainfall interception during the growing and non-growing seasons in a *Fraxinus rotundifolia* plantation located in a semiarid climate. J. Agric. Sci. Technol. 17, 145–156.
Sadeghi, S.M.M., Van Stan II, J.T., Pypker, T.G., Friesen, J., 2017. Canopy hydrometeorological dynamics across a chronosequence of a globally invasive species, *Ailanthus altissima* (Mill., tree of heaven). Agric. For. Meteorol. 240, 10–17.
Sadeghi, S.M.M., Van Stan, J.T., Pypker, T.G., Tamjidi, J., Friesen, J., Farahnaklangroudi, M., 2018. Importance of transitional leaf states in canopy rainfall partitioning dynamics. Eur. J. For. Res. 137 (1), 121–130.
Sadeghi, S.M.M., Gordon, D.A., Van Stan II, J.T., 2020. A global synthesis of throughfall and stemflow hydrometeorology. Precipitation Partitioning by Vegetation: A global synthesis. Springer International Publishing, Cham, pp. 49–70.
Sadeghi, S.M.M., Panahandeh, T., Van Stan II, J.T., Babapour, S., Friesen, J., 2023. Responses of canopy hydrometorological parameters to oak dieback in the Mediterranean sparse forest, Iran. Agric. For. Meteorol. 343, 109784.
Sadeghi, S.M.M., Epstein, J.M., Deljouei, A., Gorora, F.J., Cohen, M.J., 2024. Stand age controls canopy and soil rainfall partitioning in slash pine forests. For. Ecol. Manag. 572, 122307.
Saeedi, Z., Azadfar, D., Tohidafar, M., Sagheb-Talebi, K., 2022. Analyses of leaf morphological changes and expressed genes related to water shortage of *Fagus orientalis* populations in a drought gradient. Balt. For. 28 (2), 205.
Safe'i, R., Puspita, E.N., Hilmanto, R., 2022. Assessment of tree vitality as an indicator of monitoring the health condition of community forest in agroforestry patterns. Folia For. Pol. Ser. A. For. 64 (4), 206–213.
Sagheb Talebi, K., 2017. Close to nature silviculture; Views and goals. Iran. Nat. 2 (1), 9, 6.
Sagheb-Talebi, K., Sajedi, T., Pourhashemi, M., 2014. Forests of Iran. A Treasure A Hope Future.
Sefidi, K., 2023. Rare species impacts on structural complexity index (SCI) in the Hyrcanian beech forests. For. Res. Dev. 9 (2), 205–219.
Sefidi, K., Copenheaver, C.A., 2020. Tree-related microhabitats: a comparison of managed and unmanaged oriental beech–dominated forests in northern Iran. For. Sci. 66 (6), 747–753.
Spittlehouse, D., Maloney, D., 2023. Rainfall interception by mature coastal and interior forests in British Columbia. Confluence J. Watershed Sci. Manag. 6 (1), 20.
Su, L., Yang, J., Zhao, X., Miao, Y., 2022. Effects of fire on interception loss in a coniferous and broadleaved mixed forest. J. Hydrol. 613, 128425.
Tague, C.L., Band, L.E., 2004. RHESSys: Regional Hydro-Ecologic Simulation System—An object-oriented approach to spatially distributed modeling of carbon, water, and nutrient cycling. Earth Interact. 8 (19), 1–42.
Tang, C., 1996. Interception and recharge processes beneath a *Pinus elliotii* forest. Hydrol. Process. 10 (11), 1427–1434.
Tavankar, F., Kivi, A.R., Taheri-Abkenari, K., Lo Monaco, A., Venanzi, R., Picchio, R., 2022. Evaluation of deadwood characteristics and carbon storage under different silvicultural treatments in a mixed broadleaves mountain forest. Forests 13 (2), 259.
Tomar, J.M.S., Kar, S.K., Ahmed, A., Sankar, M., Jayaprakash, J., Kaushal, R., Islam, S., Mehta, H., Chaturvedi, O.P., 2022. Hydrological fluxes from Sal (*Shorea robusta*) forests under various disturbance gradients of Himalayan foothills. Ecohydrol. Hydrobiol. 22 (3), 541–552.
Tonello, K.C., Campos, S.D., de Menezes, A.J., Bramorski, J., Mathias, S.L., Lima, M.T., 2021. How is bark absorbability and wettability related to stemflow yield? Observations from isolated trees in the Brazilian Cerrado. Front. For. Glob. Change 4, 650665.
Valente, F., David, J.S., Gash, J.H.C., 1997. Modelling interception loss for two sparse eucalypt and pine forests in central Portugal using reformulated Rutter and Gash analytical models. J. Hydrol. 190, 141–162.
Van Dijk, A.I., Gash, J.H., Van Gorsel, E., Blanken, P.D., Cescatti, A., Emmel, C., Gielen, B., Harman, I.N., Kiely, G., Merbold, L., Montagnani, L., 2015. Rainfall interception and the coupled surface water and energy balance. Agric. For. Meteorol. 214, 402–415.
Van Stan, J.T., Simmons, J., 2025. Water models as geographical chimera: precipitation interception routines as an example of "patchwork empiricism. Water Altern. 18 (2), 240–260.
Van Stan, J.T., Gutmann, E.D., Lewis, E.S., Gay, T.E., 2016. Modeling rainfall interception loss for an epiphyte-laden Quercus virginiana forest using reformulated static-and variable-storage Gash analytical models. J. Hydrometeorol. 17 (7), 1985–1997.
Waiters, R.J., Price, A.G., 1988. The influence of stemflow from standing dead trees on the fluxes of some ions in a mixed deciduous forest. Can. J. For. Res. 18 (11), 1490–1493.
Wang, Y., Titus, S.J., LeMay, V.M., 1998. Relationships between tree slenderness coefficients and tree or stand characteristics for major species in boreal mixedwood forests. Can. J. For. Res. 28 (8), 1171–1183.
Wei, L., Qiu, Z., Zhou, G., Zuecco, G., Liu, Y., Wu, Z., 2020. Rainfall interception recovery in a subtropical forest damaged by the great 2008 ice and snow storm in southern China. J. Hydrol. 590, 125232.
Xu, X., 2023. Effect of changes in throughfall on soil respiration in global forest ecosystems: a meta-analysis. Forests 14 (5), 1037.
Yue, K., De Frenne, P., Fornara, D.A., Van Meerbeek, K., Li, W., Peng, X., Ni, X., Peng, Y., Wu, F., Yang, Y., Peñuelas, J., 2021. Global patterns and drivers of rainfall partitioning by trees and shrubs. Glob. Change Biol. 27 (14), 3350–3357.
Zamani, S.M., Sepasi, N., Afarin, S., Ahangaran, Y., Gholami Ghavam Abad, R., Askary, H., 2024. Report of *Biscogniauxia nummularia* as pathogenic agent of charcoal canker disease of beech (*Fagus orientalis*) from Iran. Iran. J. For. Range Prot. Res. 21 (2), 358, 350.